Original Article

Assessment of dynamic characteristics of thin cylindrical sandwich panels with magnetorheological core

Gennadi I Mikhasev[1] (ID), Victor A Eremeyev[2], Krzysztof Wilde[2] and
Svetlana S Maevskaya[3]

Abstract

Based on the equivalent single-layer linear theory for laminated shells, free and forced vibrations of thin cylindrical sandwich panels with magnetorheological core are studied. Five variants of available magnetorheological elastomers differing in their composition and physical properties are considered for smart viscoelastic core. Coupled differential equations in terms of displacements based on the generalized kinematic hypotheses of Timoshenko accounting for transverse shears with coefficients depending on the complex shear modulus for a smart core are used to govern vibrations of cylindrical panels. Assuming conditions of simple support for straight and curvilinear edges, solutions in the explicit form describing natural modes as well as an equation with respect to the required complex eigenfrequencies are found. To predict the shell response to an external harmonic force, the general solution of non-homogeneous governing equations is derived in the form of series in natural modes. To estimate damping capability of magnetorheological elastomers under consideration, the principle tunable parameters, the lowest natural frequencies and associated logarithmic decrements are calculated for the same panels with different magnetorheological elastomers under the action of a magnetic field of different intensities. Finally, the amplitude–frequency plots for magnetorheological elastomer-based panels of different opening angles with and without magnetic field are presented.

Keywords

Sandwich cylindrical panel, magnetorheological elastomer, natural oscillations, damping ratio, forced vibrations, amplitude–frequency plots

1. Introduction

During the last two decades, magnetorheological elastomers (MREs) became to attract a close attention of many research scholars studying and designing smart thin-walled structures with controllable viscoelastic properties (Deng et al., 2006; Jolly et al., 1996; Li et al., 2014; Shaw and Wang, 2019). These intelligent materials demonstrate very fast time response to an applied magnetic field (Sun et al., 2003), that is in the order of few milliseconds. Available experimental analysis by Yalcintas and Dai (2003), Wei et al. (2008), Lara-Prieto et al. (2009), Chikh et al. (2016), Kozlowska et al. (2016) and Irazu and Elejabarrieta (2017) and numerous theoretical studies by Yalcintas and Dai (1999), Sun et al. (2003), Zhou and Wang (2005a, 2005b, 2006a, 2006b), Hu et al. (2006), Nayak et al. (2011, 2012) and Korobko et al. (2012) on vibrations of MRE-based sandwich beams have shown that the action of magnetic field may result in the noticeable enhancement of both the total stiffness and damping

ratio of smart beams and, as a consequence, allows significant changes in the main dynamic characteristics such as natural frequencies, amplitudes, mode shapes and loss factors.

Nowadays, there are a large number of studies on free vibrations of sandwich structures, containing MRE core, such as beams and plates with zero Gaussian curvature (ZGC). These studies used various theoretical approaches and models, resulting in sometimes unexpected mechanical effects. For example, Zhou and Wang (2005b, 2006a, 2006b) and Choi et al. (2010) proposed the mathematical models based on the high-order

[1]Belarusian State University, Minsk, Belarus
[2]Gdańsk University of Technology, Gdańsk, Poland
[3]Vitebsk State University, Vitebsk, Belarus

Corresponding author:
Gennadi I Mikhasev, Belarusian State University, Nezavisimosti Avenue,
220030 Minsk, Belarus.
Email: mikhasev@bsu.by

shear deformation theory for a soft MRE core. Zhou and Wang (2006a, 2006b) accounted for normal stresses in MRE layer. The effect of non-homogeneous magnetic field on MRE sandwich beams fabricated from an MRE between two aluminium layers was examined by Hu et al. (2011, 2012) and Long et al. (2013). The majority of investigations showed that the application of a uniform magnetic field results in the increase of the total stiffness of an MRE-based sandwich beam and leads to right shift of natural frequencies. The experimental tests performed by Hu et al. (2011, 2012) revealed unlooked-for result: the first natural frequency of a cantilever MRE-beam decreased as the magnetic field applied to the beam was moved from the clamped edge to the free one. Recently, the left shift trend of the first natural frequency has been confirmed by both the finite-element simulation, see Megha et al. (2016) and other accurate experiments performed by de Souza et al. (2018, 2019).

In the literature, there are numerous studies on free vibrations of sandwich plates with embedded electrorheological (ER) or magnetorheological (MR) core. We highlight here, the papers by Yeh (2013, 2014), Aguib et al. (2014), Eshaghi et al. (2015), Babu and Vasudevan (2016) and Zhang et al. (2018). Yeh (2013, 2014) performed the vibration analysis of MRE-based isotropic and orthotropic sandwich rectangular plates. In the numerical and experimental studies by Aguib et al. (2014), the dynamic behaviour of sandwich plates consisting of two aluminium skins and a polarized MRE core have been examined. Eshaghi et al. (2015) compared the damping properties of two sandwich plates consisting of polyethylene terephthalate face layers with two different magnetorheological fluids as the core layers. Applying FEM and carrying out experiments, Babu and Vasudevan (2016) studied the effect of magnetic field on dynamic performance of tapered laminated MRE sandwich plates. Zhang et al. (2018) have performed interesting experiments to analyse non-linear vibrations of an MRE-based sandwich plate under the action of a localized magnetic field located in different points.

The vibration analysis of thin-walled structures becomes very important when the applied load is non-stationary and induces resonance vibrations as in typical situations which are widely observed in the mechanical and civil engineering. The advantages of using intelligent materials like MR liquids or MREs to suppress forced vibrations of sandwich ZGC structures were clearly demonstrated by Dwivedy et al. (2009), Rajamohan et al. (2009), Nayak et al. (2014), Aguib et al. (2016), Megha et al. (2016), Yildirim et al. (2016), Liao et al. (2011), Eshaghi et al. (2016) and Babu and Vasudevan (2016). For instance, Aguib et al. (2016) have convincingly demonstrated, both experimentally and numerically, the suppression of forced vibrations applying magnetic field in an MRE-based sandwich

beam subjected to harmonic force. Babu and Vasudevan (2016) also revealed this effect studying transverse vibrations of tapered MRE-based sandwich plates under harmonic force excitation.

For sandwich shells containing ER/MR core, there are only a few results, see, for example, Yeh (2011), Mohammadi and Sedaghati (2012), Mikhasev et al. (2011, 2014) and Altenbach et al. (2008). Yeh (2011) and Mohammadi and Sedaghati (2012) developed different variants of FEM to analyse free vibrations of sandwich shells containing ER core and shown that applying electric fields leads to both the change of eigenfrequencies and enhancement of damping properties of smart structures. The equivalent single-layer (ESL) model for laminated cylindrical shells developed by Grigolyuk and Kulikov (1988) was later adapted by Mikhasev et al. (2011) for the prediction of dynamic behaviour of laminated cylindrical shells containing MRE layers. Later, this model was used to examine the effect of magnetic field on the localized eigenmodes of a medium-length thin sandwich cylindrical shell containing a highly polarized MR core (Mikhasev et al., 2014), where it was revealed that the action of a magnetic field may result in strong distortion of the localized eigenmodes corresponding to the lowest frequencies. Let us note that the ESL models for laminate shells and plates, including sandwiches, are widely used in the engineering, see, for example, Altenbach (2000), Eisenträger et al. (2015), Altenbach et al. (2015) and Chróścielewski et al. (2011). The other models are based on more complex shell kinematics or asymptotic approaches, see, for example, Naumenko and Eremeyev (2014, 2017), Kreja (2011), Carrera (2003), Carrera et al. (2011), Giunta et al. (2013), Tovstik and Tovstik (2016), Kaplunov et al. (2017) and Prikazchikova et al. (2018).

Considering dynamics of thin-walled members made of ER/MR composites, we also underline some similarities between these structures and widely used piezoelectric beams, plates and shells, see, for example, Carrera (1997), Wang et al. (2000), Ballhause et al. (2005), Araújo et al. (2016), Abdeljaber et al. (2016), Nielsen et al. (2017) and Chróścielewski et al. (2019) and the extensive reference therein.

The above-performed analysis clearly points out the lack of detailed analysis of dynamic characteristics for thin cylindrical sandwich panels, which are mostly used as thin-walled members in airborne/space-borne vehicles and cars. The need to pay attention to cylindrical panels containing smart (ER/MR) core could be explained by the fact that mechanism of suppression of vibrations in thin cylindrical shells differs considerably from that one for ZGC structures and strongly depends on both the geometry (thickness, length, curvature, opening angle) and a number of waves in eigenmodes. A panel with a small opening angle is close in plan to the plate, which is characterized by a monotonic increase in the natural frequencies of the lower part of

spectrum with an increase in the wave number. As shown in recent book by Mikhasev and Altenbach (2019), the effect of an uniform magnetic field on the lowest natural frequency in MRE-based beams and plates turns out to be weak (excluding the case of a cantilever beam placed in a localized magnetic field). In order to 'withdraw' such smart structure from the regime of low-frequency resonance vibrations or to enhance damping properties, one needs to apply a very large uniform magnetic field. As for medium-length thin closed cylindrical shells, their low-frequency natural modes are characterized by a large number of waves in circumferential direction. The suppression of such oscillations is rather complicated, the main influential factors become both the right shifting eigenfrequencies and energy dissipation. In the light of these properties of thin cylindrical panels, the damping capability of different available MREs used as a core material becomes a subject for investigation. We intend to find out which types of MREs being different in density, storage modulus and loss factor are the most optimal for damping vibrations of a cylindrical sandwich panel taking into account its geometry (core thickness, opening angle, etc.).

Finally, let us emphasize that the effect of magnetic field on forced stationary and non-stationary vibrations of MRE-based sandwiches remains not sufficiently studied. In particular, there are a few papers analysing transient response of MRE shells based on the representation of the viscoelastic moduli in the complex form. It is explained by the fact that assuming the shell stiffness in the complex form yields additional 'spurious' complex eigenfrequencies which result in increasing amplitudes of free vibrations. As a rule, these 'eigenfrequencies' are ignored, and for considering forced vibrations, only regime of steady vibrations is analysed.

To eliminate aforementioned gaps, we apply here the ESL theory for MRE-based laminated shells accounting for transverse shear to predict vibrations of cylindrical sandwich panels assembled from various MREs differing in compositions and their viscoelastic properties. First, using the kinematic hypotheses, strain–displacement relations and constitutive equations proposed by Grigolyuk and Kulikov (1988) for laminated shells, we briefly derive the governing equations with coefficients depending on the complex shear modulus in terms of displacements and shears. These equations can describe damped vibrations of cylindrical MRE panels of any geometry under the action of both edge or surface forces. Then, the basic attention is paid to study the effect of magnetic field on the lowest natural frequencies and on associated logarithmic decrements for panels with different opening angles, smart core thicknesses and containing various MREs. In order to predict the non-stationary response of the MRE-based sandwich panel to the periodic force excitation, we propose new mathematical model. It is based on replacing the initial governing equations by the series of so-called 'equivalent oscillators' with external friction resulting in the same set of natural frequencies and associated decrements. Finally, the amplitude–frequency response of smart cylindrical panels with different geometrical parameters and various MREs under the action of concentrated periodic forces is also examined.

2. Structure of smart sandwich cylindrical panel

2.1. Geometrical dimensions and components of a sandwich

We consider a thin three-layered circular cylindrical sandwich panel of the length L_1 and width L_2, as shown in Figure 1. It is assumed that L_1 and L_2 are of the same order ($L_1 \sim L_2$). Each layer is characterized by thickness h_k, mass density ρ_k, Young's modulus E_k, shear modulus G_k and Poisson's ratio ν_k, where $k = 1$ and $k = 3$ denote the bottom and upper faces, respectively, and $k = 2$ corresponds to the core made of a smart material.

The face sheets are made of an elastic material which is not affected by an external magnetic field and assumed to be isotropic. For this material, E_1 and E_3 are real numbers. The smart core is fabricated from a viscoelastic material, MRE. In what follows, we consider several different MREs, which properties are available in the literature. Accordingly, smart sandwiches assembled from these MREs will be studied below.

The middle surface of the core is taken as the original one with the radius of curvature R. The coordinate system, α_1 and α_2, is given in Figure 1, where α_1 and α_2 are the axial and circumferential coordinates, respectively. We also introduce the opening angle of the panel, given by $\varphi_2 = L_2/R$.
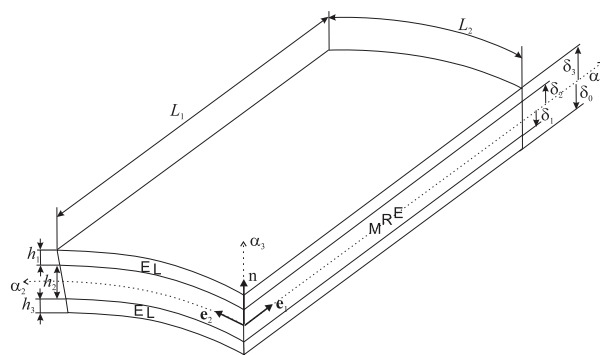

Figure 1. Thin sandwich cylindrical panel consisting of elastic layers (EL) and the smart core made of MRE. Curvilinear coordinate system is at the original surface.

2.2. MREs and their viscoelastic properties

The basic components of any MRE are a non-magnetic matrix and magnetizable particles moulded in this matrix. As a matrix, elastomeric or rubber-like materials (Farshad and Benine, 2004; Li et al., 2010; Wang et al., 2009) including naturally deformed polymers (Farshad and Benine, 2004), natural rubbers (Yang et al., 2013) and synthetic ones (Bica et al., 2014; Sun et al., 2008; Wang et al., 2006) are used. The elastic and rheological properties of these smart materials strongly depend on both composition and ratio of all components. The optimum weight/density ratio of magnetic particles, carrier viscous liquid, polymer matrix and additional components substantially determines shear modulus and viscosity of MRE.

In the case of harmonic (sinusoidal) response of MREs, their properties are, as a rule, represented by complex Young's and shear moduli. So, regardless of the type of MRE used below for the core, we assume that

$$E_2 = E_2' + iE_2'', \quad G_2 = G_2' + iG_2'', \quad i = \sqrt{-1} \quad (1)$$

where G_2' and G_2'' are called the storage and loss moduli, respectively. In general case, the moduli E_2 and G_2 are considered as independent magnitudes. For example, Aguib et al. (2014) assumed that Young's modulus E_2 and Poisson's ratio ν_2 are independent real parameters which are not affected by a magnetic field. If MRE is assumed to be an isotropic material, then E_2 and G_2 are coupled, $G_2 = E_2/[2(1 + \nu_2)]$, where Poisson's ratio ν_2 is a real number.

It is of interest to note that the first representation of stiffness in the complex form was given by Soroka (1949). Utilizing observations by Kimball and Lovell (1927) for many engineering viscoelastic damping materials, Soroka has proposed to replace the stiffness k in the undamped elastic system by the Kimball–Lovell *complex stiffness*, $k = k' + ik''$. Since then, viscoelastic models based on the complex representation of Young's and/or shear moduli have been intensively used to predict stationary response of viscoelastic structures with internal friction, see early papers by Kerwin (1959) and Ross et al. (1959) or recently issued studies by Korobko et al. (2012), Nayak et al. (2012) and Aguib et al. (2014) and the comprehensive review by Eshaghi et al. (2016) on vibrations of MRE-based laminated structures.

For a majority of available MREs, the functional dependencies of the storage and loss moduli on the magnetic field induction B are much affected by both the frequency of vibrations, amplitude of shear deformations (Kwon et al., 2018) and the sample thickness as well. However, under high-frequency excitation of small harmonic deformations of a sufficiently thick sample of MRE, functions $G_2'(B)$ and $G_2''(B)$ display almost the same behaviour. For all MREs to be considered below, the storage and loss moduli may be assumed as invariants with respect to the frequency of small vibrations if this frequency exceeds 10 Hz.

As the sandwich core, we shall consider five samples of MREs whose elastic and rheological properties are available: MRE-1 elaborated by Korobko et al. (2012), MRE-2 by Aguib et al. (2014), MRE-3, MRE-4 and MRE-5 proposed by Chen et al. (2008). These elastomers are different in composition and, as consequence, have different properties. We note that MRE-1 is almost two times heavier than MRE-2 and about 1.4 times heavier than others. Viscoelastic properties of these MREs are listed in Appendix 1, MRE-2 being considered as the four-parameter viscoelastic material with the real Young's modulus E_2 and Poisson's ratio ν_2 independent of a magnetic field, while the others being treated as isotropic ones. It is also assumed that the thickness of any MRE core is sufficient and do not influence on the storage and loss moduli of the MRE itself.

When comparing briefly properties of the aforementioned MREs, one can conclude that more heavier elastomer MRE-1 possess the largest loss factor without magnetic field, however under the action of a magnetic field, its loss factor dramatically drops. We also notice that the MRE-5 with the highest content of carbon black has very large shear moduli with respect to other considered MREs. It is also of interest to note that adding carbon black results in the weak dependence of the loss factor on the magnetic field induction. These unique properties inherent in each of the elastomers should be taken into account when designing intelligent sandwiches with controlled viscoelastic properties.

3. Equivalent single-layer shell model for thin-walled smart sandwich structures

We follow the approach developed by Grigolyuk and Kulikov (1988), according to which the dynamic behaviour of a thin-layered transversally isotropic shell may, under certain conditions, be predicted using the theory of equivalent single-layer shells. The use of this approach for laminated shells containing MREs was proposed by Mikhasev et al. (2011) and further by Mikhasev and Altenbach (2019). Note that the equivalent homogeneous models of plates and shells are widely used in the literature, see, for example, Altenbach et al. (2015) and the reference therein.

3.1. Basic hypotheses

Let $\alpha_3 = \delta_k$ be a coordinate of the upper bound of the k th layer, and $\alpha_3 = \delta_0$ be a coordinate of the inner surface of the shell, as shown in Figure 1. We introduce the following notations u_1, u_2 and w, which are the

axial, circumferential and normal displacements of a point at the reference surface, respectively, $u_1^{(k)}$ and $u_2^{(k)}$ are the tangential displacements of a point laying at the kth layer middle surface, $\bar{\sigma} = (\sigma_{11}, \sigma_{22}, \sigma_{12})^{\mathrm{T}}$ and $\bar{\sigma}_3 = (\sigma_{13}, \sigma_{23})^{\mathrm{T}}$ are the vectors of tangential (with respect to the original surface) and transverse shear stresses, respectively, and $\bar{\epsilon} = (\epsilon_{11}, \epsilon_{22}, \epsilon_{12})^{\mathrm{T}}$ and $\bar{\epsilon}_3 = (\epsilon_{13}, \epsilon_{23})^{\mathrm{T}}$ are the associated vectors of strains, θ_i is the angle of rotation of the normal **n** about the vector $\mathbf{e}_i$ (see Figure 1). Here, $i = 1, 2; k = 1, 2, 3$.

Following Grigolyuk and Kulikov (1988), we summarize here the basic hypotheses of the laminated shell theory:

- The distribution law of the transverse shear stresses across the thickness of the kth layer is assumed to be of the form

$$\sigma_{i3} = f_0(\alpha_3)\mu_i^{(0)}(\alpha_1, \alpha_2, t) + f_k(\alpha_3)\mu_i^{(k)}(\alpha_1, \alpha_2, t) \quad (2)$$

where t is time, and $f_0(\alpha_3)$ and $f_k(\alpha_3)$ are continuous functions introduced as follows

$$f_0(\alpha_3) = \frac{(\alpha_3 - \delta_0)(\delta_N - \alpha_3)}{h^2} \text{ for } \alpha_3 \in [\delta_0, \delta_N]$$

$$f_k(\alpha_3) = \frac{(\alpha_3 - \delta_{k-1})(\delta_k - \alpha_3)}{h_k^2} \text{ for } \alpha_3 \in [\delta_{k-1}, \delta_k] \quad (3)$$

$$f_k(\alpha_3) = 0 \text{ for } \alpha_3 \notin [\delta_{k-1}, \delta_k]$$

- Normal stresses acting on the area elements parallel to the original one are negligible with respect to other components of the stress tensor.
- The normal deflection $w(\alpha_1, \alpha_2, t)$ does not depend on the coordinate α_3.
- The tangential displacements are distributed across thickness of the layer package according to the generalized kinematic Timoshenko hypothesis

$$u_i^{(k)}(\alpha_1, \alpha_2, \alpha_3, t) = u_i(\alpha_1, \alpha_2, t) - \alpha_3 w_{,i}(\alpha_1, \alpha_2, t) + g(\alpha_3)\psi_i(\alpha_1, \alpha_2, t) \quad (4)$$

where $g(\alpha_3) = \int_0^{\alpha_3} f_0(x)\mathrm{d}x, k = 1, 2, 3$.

In equation (4), ψ_i is the parameter characterizing the transverse shears, and the subindex i followed by comma means the differentiation with respect to the coordinate α_i. Hypothesis (4) permits to describe the non-linear dependence of the tangential displacements on α_3; at $g \equiv 0$ it turns into the linear Timoshenko hypothesis coinciding with the classical Kirchhoff–Love hypothesis. The functions $\mu_i^{(0)}$ and $\mu_i^{(k)}$ are coupled with the vector $\bar{\Psi} = (\psi_1, \psi_2)^T$ and depend on elements of a matrix characterizing the transverse shear deformability of the kth layer (for more detail, we refer to the book by Grigolyuk and Kulikov (1988)).

3.2. Strain–displacement relations

The strain–displacement relations are assumed as follows

$$\epsilon_{ij} = e_{ij} + z\,\kappa_{ij} + g(z)\psi_{ij}, \; \epsilon_{i3} = f_0(z)\psi_i \quad (5)$$

where

$$e_{ij} = \frac{1}{2}(u_{i,j} + u_{j,i} + w_{,i}w_{,j}) + k_{ij}w$$

$$\psi_{ij} = \frac{1}{2}(\psi_{i,j} + \psi_{j,i}), \quad \kappa_{ij} = -w_{ij}, \quad i,j = 1, 2 \quad (6)$$

$$k_{11} = k_{12} = 0, \quad k_{22} = 1/R$$

with κ_{ii} and κ_{12} characterizing the bending and twisting deformations of the original surface.

3.3. Constitutive equations

When taking into account the static hypothesis (2) for the transverse shear stresses, the vectors of tangential stresses $\bar{\sigma}$ and associated vector of strains $\bar{\epsilon}$ are linked by Hooke's law

$$\sigma_{ij} = \frac{E_k}{1 - \nu_k^2}\Xi\epsilon_{ij}, \quad i,j = 1, 2 \quad (7)$$

where

$$\Xi\epsilon_{ij} = (1 - \nu)\epsilon_{ij} + \nu\delta_{ij}(\epsilon_{11} + \epsilon_{22}) \quad (8)$$

δ_{ij} is the Kronecker symbol $(\delta_{ii} = 1; \delta_{ij} = 0, i \neq j)$, while the transverse shear stresses are assumed to satisfy the following constitutive equation

$$\bar{\epsilon}_3 = \mathbf{A}_3^{(k)}\bar{\sigma}_3, \quad k = 1, 2, 3 \quad (9)$$

Here

$$\mathbf{A}_3^{(k)} = \begin{pmatrix} a_{55}^{(k)} & a_{45}^{(k)} \\ a_{45}^{(k)} & a_{44}^{(k)} \end{pmatrix} \quad (10)$$

is the 2×2 matrix of the transverse shear compliances. For an isotropic layer, $a_{45}^{(k)} = 0, a_{55}^{(k)} = a_{44}^{(k)} = G_k^{-1}$ with G_2 being complex for the smart MRE core.

Let us note that within the assumed ESL model for a sandwich, due to hypothesis (2), the constitutive equation (9) does not hold. However, as will be shown below, it is satisfied integrally with some weight function for the thickness of the laminated package.

3.4. Variational principle

Applying the mixed variational principle for a static problem, Grigolyuk and Kulikov (1988) derived the equilibrium equations for laminated elastic shells in terms of the stress resultants. Here, we consider the dynamic problem when the cylindrical panel is under

dynamic load with $q_i(\alpha_j, t)$ and $q_3(\alpha_j, t)$ being the components of surface tangential and normal forces, respectively. In the general case, the panel may also be subjected by an edge load. Let $\mathcal{L}$ be the Lagrangian of the system

$$\mathcal{L} = \mathcal{K} - \Pi \qquad (11)$$

where

$$\mathcal{K} = \frac{1}{2} \sum_{k=1}^{3} \rho_k h_k \iint_{\mathcal{D}} \left(\sum_{i=1}^{2} \dot{u}_i^2 + \dot{w}^2 \right) d\alpha_1 d\alpha_2 \qquad (12)$$

is the kinetic energy, and

$$\Pi = \iint_{\mathcal{D}} \left[\sum_{k=1}^{3} \int_{\delta_{k-1}}^{\delta_k} (\bar{\sigma}^{\mathrm{T}} \bar{\epsilon} + \bar{\sigma}_3^{\mathrm{T}} \epsilon_3 W_k) \quad \times (1 + k_{22}z) dz \right] d\alpha_1 d\alpha_2 - \mathcal{A}_f \qquad (13)$$

is the total potential energy of the system with $\mathcal{A}_f$ being the work of external forces (it is not give here). Also

$$W_k = \frac{1}{2} \left(\bar{\sigma}^{\mathrm{T}} \mathbf{A}^{(k)} \bar{\sigma} + \bar{\sigma}_3^{\mathrm{T}} \mathbf{A}_3^{(k)} \bar{\sigma}_3 \right) \qquad (14)$$

denotes the strain-energy function of the kth layer, $\mathcal{D}$ is the domain of the panel reference surface, and

$$\mathbf{A}^{(k)} = \begin{pmatrix} a_{11}^{(k)} & a_{12}^{(k)} & a_{16}^{(k)} \\ a_{12}^{(k)} & a_{22}^{(k)} & a_{26}^{(k)} \\ a_{16}^{(k)} & a_{26}^{(k)} & a_{66}^{(k)} \end{pmatrix} \qquad (15)$$

is the 3×3 matrix of the plane compliances for the kth layer with the elements

$$a_{11}^{(k)} = a_{22}^{(k)} = \frac{1}{E_k}, \quad a_{12}^{(k)} = -\frac{\nu_k}{E_k},$$
$$a_{66}^{(k)} = \frac{1 + \nu_k}{E_k}, \quad a_{16}^{(k)} = a_{26}^{(k)} = 0 \qquad (16)$$

Note that in the functional Π, the components of deformation and transverse shear stresses are considered as independent variable functions.

3.5. Governing equations and boundary conditions

Equating the first variation of the action functional

$$\mathcal{A} = \int_{t_1}^{t_2} \mathcal{L} dt$$

to zero, and accounting for the above strain–displacement and constitutive equation, we arrive at the following system of five differential equations

$$\hat{u}_{1,11} + \frac{1-\nu}{2} \hat{u}_{1,22} + \frac{1+\nu}{2} \hat{u}_{2,12} + \frac{1}{R} w_{,1} = -\frac{(1-\nu^2)}{Eh} \left(q_1 - \sum_{k=1}^{3} \rho_k h_k \frac{\partial^2 \hat{u}_1}{\partial t^2} \right)$$

$$\frac{1+\nu}{2} \hat{u}_{1,12} + \frac{1-\nu}{2} \hat{u}_{2,11} + \hat{u}_{2,22} + \frac{1}{R} w_{,2} = -\frac{(1-\nu^2)}{Eh} \left(q_2 - \sum_{k=1}^{3} \rho_k h_k \frac{\partial^2 \hat{u}_2}{\partial t^2} \right)$$

$$\eta_2 \Delta w_{,1} - \eta_1 \left(\psi_{1,11} + \frac{1+\nu}{2} \psi_{2,12} + \frac{1-\nu}{2} \psi_{1,22} \right) + \frac{12(1-\nu^2)q_{44}}{Eh^3} \psi_1 = 0 \qquad (17)$$

$$\eta_2 \Delta w_{,2} - \eta_1 \left(\psi_{2,22} + \frac{1+\nu}{2} \psi_{1,12} + \frac{1-\nu}{2} \psi_{2,11} \right) + \frac{12(1-\nu^2)q_{44}}{Eh^3} \psi_2 = 0$$

$$\frac{h^2}{12(1-\nu^2)} \Delta \left[\eta_3 \Delta w - \eta_2 (\psi_{1,1} + \psi_{2,2}) \right] + \frac{1}{R(1-\nu^2)} \left(\nu \hat{u}_{1,1} + \frac{w}{R} \right) = \frac{1}{Eh} \left(q_3 - \frac{1}{2} hc_{13} \sum_{i=1}^{2} q_{i,i} - \sum_{k=1}^{3} \rho_k h_k \frac{\partial^2 w}{\partial t^2} \right)$$

with respect to five displacements $w, \hat{u}_1, \hat{u}_2, \psi_1,$ and ψ_2, the equations coupling the transverse shear stresses with the shear strains are

$$\int_{\delta_{k-1}}^{\delta_k} \left(\bar{\epsilon}_3 - \mathbf{A}_3^{(k)} \bar{\sigma}_3 \right) f_k(z) dz = 0, \quad k = 1, 2, 3$$
$$\sum_{k=1}^{3} \int_{\delta_{k-1}}^{\delta_k} \left(\epsilon_3 - \mathbf{A}_3^{(k)} \bar{\sigma}_3 \right) f_0(z) dz = 0 \qquad (18)$$

and the natural boundary conditions. Here, we consider only the one variant of boundary conditions, the conditions of simply supported edges, $\alpha_1 = 0, L_1$ and $\alpha_2 = 0, L_2$, with diaphragms preventing shears at the edge planes. In terms of displacements, stress resultants and stress couples, they read (Mikhasev and Altenbach, 2019)

$$w = \hat{u}_2 = \psi_2 = 0$$
$$\hat{M}_{11} = \eta_3(w_{,11} + \nu w_{,22}) - \eta_2(\psi_{1,1} + \nu \psi_{2,2}) = 0$$
$$T_{11} = \hat{u}_{1,1} + \nu \hat{u}_{2,2} + \nu R^{-1} w = 0 \qquad (19)$$
$$\hat{L}_{11} = \eta_2(w_{,11} + \nu w_{,22}) - \eta_1(\psi_{1,1} + \nu \psi_{2,2}) = 0$$

at $\alpha_1 = 0, L_1$ and

$$w = \hat{u}_1 = \psi_1 = 0$$
$$\hat{M}_{22} = \eta_3(w_{,22} + \nu w_{,11}) - \eta_2(\psi_{2,2} + \nu \psi_{1,1}) = 0$$
$$T_{22} = \hat{u}_{2,2} + \nu \hat{u}_{1,1} + R^{-1} w = 0 \qquad (20)$$
$$\hat{L}_{22} = \eta_2(w_{,22} + \nu w_{,11}) - \eta_1(\psi_{2,2} + \nu \psi_{1,1}) = 0$$

for $\alpha_1 = 0, L_2$, where T_{11} and T_{22} are the axial and hoop membrane stress resultants, respectively, and $\hat{M}_{ii}$ and $\hat{L}_{ii}$ are the reduced bending and generalized twisting stress couples, respectively. If a shell is closed in the circumferential direction ($\varphi_2 = 2\pi$), then condition (20) is replaced by the periodicity conditions. The homogeneous conditions (19) and (20) may be generalized in order to consider an action of external edge loads. For instance, assigning $T_{ii} = T_{ii}^*(\alpha_j, t)$ for $\alpha_i = 0, L_i$, where $i, j = 1, 2, i \neq j$, and T_{11}^* and T_{22}^* are the given dynamic axial and hoop stress resultants, one has the panel subjected to the edge load.

It should be noted that for simply supported edges without diaphragms, the appropriated boundary conditions become more complicated. The influence of boundary conditions on buckling of laminated cylindrical shells was studied by Mikhasev and Botogova (2017). In particular, it has been shown that the absence of the edge diaphragms accounts for the appearance of the edge transverse shears which strongly affect the critical pressure for shear-pliable laminated shell. Depending on assumed boundary conditions and ratio between stiffness of faces and core, the layer-wise theories of plates and shells could be more precise, see Naumenko and Eremeyev (2014, 2017).

In addition, here, we have introduced the Laplace operator given by

$$\Delta = \frac{\partial^2}{\partial \alpha_1^2} + \frac{\partial^2}{\partial \alpha_2^2}$$

the generalized tangential displacements

$$\hat{u}_i = u_i - \frac{1}{2} h c_{13} w_{,i} + \frac{1}{2} h c_{12} \psi_i \qquad (21)$$

and

$$h = \sum_{k=1}^{3} h_k, \quad \nu = \sum_{k=1}^{3} \frac{E_k h_k \nu_k}{1 - \nu_k^2} \left(\sum_{k=1}^{N} \frac{E_k h_k}{1 - \nu_k^2} \right)^{-1}$$
$$E = \frac{1 - \nu^2}{h} \sum_{k=1}^{3} \frac{E_k h_k}{1 - \nu_k^2}, \quad G = q_{44}/h \qquad (22)$$

are the total thickness, reduced Poisson's ratio, Young's modulus and shear modulus, respectively, with ν, E, G being the complex functions of the magnetic field induction. Parameter q_{44} as well as other complex coefficients appearing in the governing equation (17) and boundary conditions (19) and (20) are given in Appendix 2.

Returning to the constitutive equation (9), we note that due to the derived relation (18), they hold true in integral sense with the weight functions $f_k(z)$ and $f_0(z)$ for each layer and for the entire panel thickness, respectively.

Governing equation (17) can be used to predict any class of vibrations (transverse, tangential, quasi-transverse, etc.), with any number of waves in thin cylindrical panels of any opening angle. Thus, they generalize the previously derived dynamic equations of the technical ESL theory by Grigolyuk and Kulikov (1988), which are valid for vibrations accompanied by formation of a large number of waves at least in one direction.

3.6. On the error of governing equations

The accurate estimation of an error of the ESL model for multi-layered shells is a difficult problem and remains unsolved. One of the options to verify it is to compare the analytical solutions obtained on the base of this theory with results of finite-element simulations. The calculation of natural frequencies for a sandwich cylindrical shell with aluminium face layers and epoxy core, performed on the basis of the ESL approach and finite-element method, has shown very close coincidence of results for modes with a large number of waves in the circumferential direction (Mikhasev et al., 2001). In particular, the divergence of results turned out to be minimum for medium-length thin shells and modes corresponding to low-frequency vibrations.

Another necessary requirement influencing the error of the approach concerns the order of stiff characteristics of all layers composing the sandwich. One of the principle parameters affecting the error of our ESL model is the dimensionless stiffness

$$\gamma_k = \frac{E_k h_k}{1 - \nu_k^2} \left(\sum_{k=1}^{N} \frac{E_k h_k}{1 - \nu_k^2} \right)^{-1} \qquad (23)$$

of the kth layer. To minimize the total error, the geometrical and physical parameters of layers should be chosen in such away that parameter $|\gamma_k|$ was approximately the same for all $k = 1, 2, 3$. This condition becomes essential for shells assembled from elastic and more soft viscoelastic layers.

As an example, we estimate here the parameter $|\gamma_k|$ for two 3-layered sandwiches having the same thicknesses of layers and made of different MREs. Let the top and bottom of both sandwiches be made of the ABS-plastic SD-0170 with parameters $E_1 = E_3 = 1.5 \times 10^9$ Pa, $\nu_1 = \nu_3 = 0.4$, and cores are fabricated from the MRE-1 and MRE-5, respectively. The viscoelastic properties of these materials are specified in Appendix 1. Figures 2 and 3 show the parameters $|\gamma_1| = |\gamma_3|, |\gamma_2|$ for both samples versus the magnetic induction B at the fixed thickness $h_1 = h_3 = 0.5$ mm of the elastic top and bottom layers and different thicknesses $h_2 = 3$, 5, 8, and 11 mm of the viscoelastic cores. It is seen that at a small level of magnetic field, the parameter $|\gamma_k|$ differs appreciably for both cases, and with
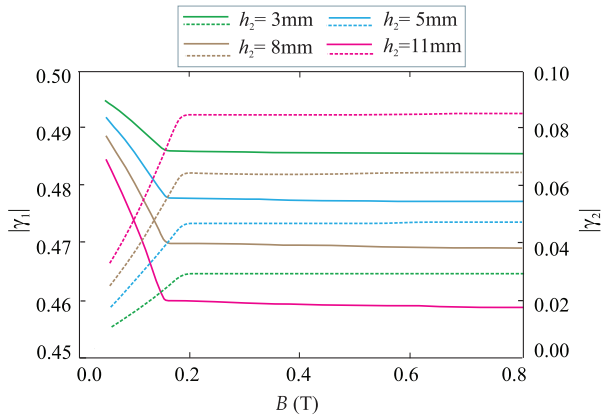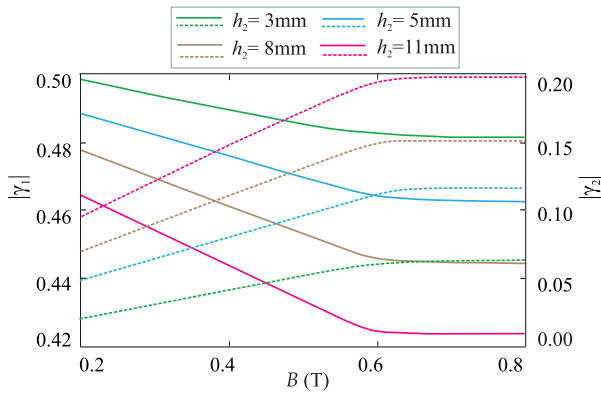
Figure 2. Dimensionless stiffness parameters $|\gamma_1| = |\gamma_3|$ (solid lines) and $|\gamma_2|$ (dotted lines) versus magnetic field induction B (T) at different thicknesses h_2 of the MRE-1 core.

Figure 3. Dimensionless stiffness parameters $|\gamma_1| = |\gamma_3|$ (solid lines) and $|\gamma_2|$ (dotted lines) versus magnetic field induction B (T) at different thicknesses h_2 of the MRE-5 core.

the increase of induction B (from 0 to 200 mT for MRE-1 and from 200 to 800 mT for MRE-5), plots for $|\gamma_1|$, $|\gamma_3|$ and $|\gamma_2|$ approach to each other, from above and below, respectively. The rise of the core thickness (under the fixed thicknesses of outer and innermost layers) also affects the stiff characteristics γ_k: the larger h_2 is, the faster values of $|\gamma_1|$, $|\gamma_3|$ and $|\gamma_2|$ approach each other with increasing magnetic field. When comparing two types of MREs, one can conclude: for the MRE-5-based sandwich, condition $|\gamma_1| = |\gamma_3| \sim |\gamma_2|$ is satisfied better, whereas for the sample with the MRE-1-based core, this requirement can be reached by only further increment in the core thickness.

As concerns the formal asymptotic estimates of the error of equation (17) and other simplified equations, they are in detail discussed in the book by Mikhasev and Altenbach (2019). We remind that these equations for elastic shells are asymptotically incorrect if moduli

E and G are of the same order ($E \sim G$ as $h_* = h/R \to 0$). However, if

$$G_r \ll E_r \qquad (24)$$

where $E_r = \Re E$, $G_r = \Re G$ are the real parts of the effective complex moduli E, G, respectively, then equation (17) become asymptotically correct. In what follows, $\Re$ and $\Im$ denote the real and imaginary parts, respectively. Below, we consider smart materials and geometrical dimensions which guarantee the fulfilment of condition (24).

4. Free-bending vibrations

Let us consider free-bending vibrations of the circular cylindrical sandwich panels. For $q_i = q_n = 0$, equation (17) with the boundary conditions (19) and (20) admit the following solution

$$
\begin{aligned}
\hat{u}_1 &= u_1^\circ \cos\frac{\pi n \alpha_1}{L_1} \sin\frac{\pi m \alpha_2}{L_2} \exp(i\Omega t) \\
\hat{u}_2 &= u_2^\circ \sin\frac{\pi n \alpha_1}{L_1} \cos\frac{\pi m \alpha_2}{L_2} \exp(i\Omega t) \\
w &= w^\circ \sin\frac{\pi n \alpha_1}{L_1} \sin\frac{\pi m \alpha_2}{L_2} \exp(i\Omega t) \qquad (25) \\
\psi_1 &= \psi_1^\circ \cos\frac{\pi n \alpha_1}{L_1} \sin\frac{\pi m \alpha_2}{L_2} \exp(i\Omega t) \\
\psi_2 &= \psi_2^\circ \sin\frac{\pi n \alpha_1}{L_1} \cos\frac{\pi m \alpha_2}{L_2} \exp(i\Omega t)
\end{aligned}
$$

where $\Omega = \omega + i\alpha$ is the complex eigenvalue, $\omega = \Re\Omega$ is the required natural frequency and $\alpha = \Im\Omega$ is the associated damping ratio which is assumed to be a positive number, n and m are numbers of semi-waves in the axial and circumferential directions, respectively, and u_i°, w°, and ψ_i° are constants. For a shell closed in the circumferential direction, a number m is assumed to be even.

When studying free-bending vibrations, the inertia terms in the first two equations from equation (17) can be omitted. Then, substituting equation (25) into equation (17), we arrive at the linear system of five algebraic equations

$$\mathbf{C}\mathbf{X}^{\mathrm{T}} = 0 \qquad (26)$$

where $\mathbf{X} = (u_1^\circ, u_2^\circ, w^\circ, \psi_1^\circ, \psi_2^\circ)$ is the amplitude vector, and $\mathbf{C}$ is the 5×5 matrix with the complex dimensionless elements c_{sr} given in Appendix 3. Equation (26) serves to find the two complex eigenvalue $\Omega = \pm(\omega + i\alpha)$ depending on the wave numbers n, m, where $\alpha > 0$. It is obvious that the second one, $\Omega = -(\omega + i\alpha)$), does not satisfy the condition of damped vibrations.

The amplitudes of tangential and shear displacements are coupled with the normal displacement as follows

$$u_1^\circ = b_1(n,m)w^\circ, \quad u_2^\circ = b_2(n,m)w^\circ$$

$$\psi_1^\circ = d_1(n,m)w^\circ, \quad \psi_2^\circ = d_2(n,m)w^\circ$$

$$b_1(n,m) = \frac{c_{13}c_{22} - c_{12}c_{23}}{c_{12}c_{21} - c_{22}c_{11}}$$

$$b_2(n,m) = \frac{c_{23}c_{11} - c_{13}c_{21}}{c_{12}c_{21} - c_{22}c_{11}} \tag{27}$$

$$d_1(n,m) = \frac{c_{33}c_{45} - c_{35}c_{43}}{c_{44}c_{35} - c_{34}c_{45}}$$

$$d_2(n,m) = \frac{c_{43}c_{34} - c_{44}c_{33}}{c_{44}c_{35} - c_{34}c_{45}}$$

where b_j and d_j are the functions of a number of semi-waves n and m in the axial and circumferential directions.

Coefficients of equation (26) depend on the following six complex parameters (see Appendix 2)

$$\eta_1, \eta_2, \eta_3, E, q_{44}, \nu \tag{28}$$

which are functions of the magnitude of an applied magnetic field. In the framework of ESL theory, they can be considered as independent integral characteristics of variable viscoelastic properties regardless of a number of layers and their properties. It is of interest to note that their number is equal to the number of independent physical characteristics of a three-layer shell (sandwich) in the case when each layer is isotropic. It has been shown by Mikhasev et al. (2014) that the reduced complex shear modulus $G = q_{44}/h$ is the basic tunable parameter influencing the complex eigenfrequency Ω, and the effect of the others on the dynamic characteristics turns out to be weak. The detailed analysis of the impact of magnetic field on parameters in equation (28) for sandwiches containing different available smart materials are given in the book by Mikhasev and Altenbach (2019).

5. Forced vibrations

Let us consider the response of the sandwich to the external normal periodical force

$$q_3(\alpha_1, \alpha_2, t) = q_3^+(\alpha_1, \alpha_2)e^{i\omega_e t} + q_3^-(\alpha_1, \alpha_2)e^{-i\omega_e t} \tag{29}$$

where ω_e is the frequency of excitation and $q_3^\pm$ is some complex dimensionless amplitude function. The combination of real and complex parts of equation (29) allows assigning any distribution of the external periodic load with the frequency ω_e.

We seek solutions of equation (17) in the form of double series

$$\hat{u}_1 = R \sum_{n=1}^{\infty} \sum_{m=1}^{\infty} U_{nm}^{(1)}(t) \cos\frac{\pi n\alpha_1}{L_1}\sin\frac{\pi m\alpha_2}{L_2}$$

$$\hat{u}_2 = R \sum_{n=1}^{\infty} \sum_{m=1}^{\infty} U_{nm}^{(2)}(t) \sin\frac{\pi n\alpha_1}{L_1}\cos\frac{\pi m\alpha_2}{L_2}$$

$$w = R \sum_{n=1}^{\infty} \sum_{m=1}^{\infty} W_{nm}(t) \sin\frac{\pi n\alpha_1}{L_1}\sin\frac{\pi m\alpha_2}{L_2} \tag{30}$$

$$\psi_1 = \sum_{n=1}^{\infty} \sum_{m=1}^{\infty} \Psi_{nm}^{(1)}(t) \cos\frac{\pi n\alpha_1}{L_1}\sin\frac{\pi m\alpha_2}{L_2}$$

$$\psi_2 = \sum_{n=1}^{\infty} \sum_{m=1}^{\infty} \Psi_{nm}^{(2)}(t) \sin\frac{\pi n\alpha_1}{L_1}\cos\frac{\pi m\alpha_2}{L_2}$$

where $U_{nm}^{(j)}(t), W_{nm}(t)$ and $\Psi_{nm}^{(j)}(t)\,(j = 1, 2)$ are the required functions of t called as the generalized coordinates of the system. The functions $q_3^\pm(\alpha_1, \alpha_2)$ are also expanded into the series

$$q_3^\pm = \sum_{n=1}^{\infty} \sum_{m=1}^{\infty} q_{nm}^\pm \sin\frac{\pi n\alpha_1}{L_1}\sin\frac{\pi m\alpha_2}{L_2} \tag{31}$$

where

$$q_{nm}^\pm = \frac{4}{L_1 L_2} \int_0^{L_1} \int_0^{L_2} q_3^\pm \sin\frac{\pi n\alpha_1}{L_1}\sin\frac{\pi m\alpha_2}{L_2} \,\mathrm{d}\alpha_1 \mathrm{d}\alpha_2 \tag{32}$$

We substitute equations (30) and (31) into the governing equation (17), then multiply them from the first to fifth by the factors

$$\cos\frac{\pi i\alpha_1}{L_1}\sin\frac{\pi j\alpha_2}{L_2}, \quad \sin\frac{\pi i\alpha_1}{L_1}\cos\frac{\pi j\alpha_2}{L_2},$$

$$\sin\frac{\pi i\alpha_1}{L_1}\sin\frac{\pi j\alpha_2}{L_2}, \quad \cos\frac{\pi i\alpha_1}{L_1}\sin\frac{\pi j\alpha_2}{L_2}, \quad \sin\frac{\pi i\alpha_1}{L_1}\cos\frac{\pi j\alpha_2}{L_2}$$

respectively, where i and j are fixed natural numbers, and then, finally, integrate them over the panel surface. As a result, eliminating $U_{nm}^{(s)}(t)$ and $\Psi_{nm}^{(s)}(t)\,(s = 1, 2)$ from the first four equations, we arrive at the differential equation

$$\ddot{W}_{ij}^\pm + \Omega_{ij}^2 W_{ij}^\pm = \frac{q_{ij}^\pm}{\rho_0 hR}e^{\pm i\omega_e t}, \quad i, j = 1, 2, \ldots \tag{33}$$

with respect to the function $W_{ij}^\pm(t)$, where $\Omega_{ij} = \pm(\omega + i\alpha)$ is the complex eigenfrequency determined from equation (26).

5.1. Steady-state forced vibrations

The partial solutions of equation (33) read

$$W_{ij}^\pm(t) = \frac{q_{ij}^\pm}{\rho_0 hR(\Omega_{ij}^2 - \omega_e^2)}e^{\pm i\omega_e t} \tag{34}$$

Then, the steady-state forced vibrations at any point on the panel surface will be defined by the formula

$$w = R \sum_{n=1}^{\infty} \sum_{m=1}^{\infty} \frac{q_{nm}^+ e^{i\omega_e t} + q_{nm}^- e^{-i\omega_e t}}{\rho_0 hR(\Omega_{nm}^2 - \omega_e^2)} \times \sin\frac{\pi n\alpha_1}{R}\sin\frac{\pi m\alpha_2}{R} \tag{35}$$

and the associated displacements $\hat{u}^{(1)}, \hat{u}^{(2)}, \psi^{(1)}$ and $\psi^{(2)}$ are calculated by equation (30), where

$$U_{nm}^{(s)}(t) = b_s(n,m)\tilde{W}_{nm}(t)$$

$$\Psi_{nm}^{(s)}(t) = d_s(n,m)\tilde{W}_{nm}(t) \quad s = 1, 2$$

Formula (35) allows us to determine such important dynamic characteristic as the amplitude–frequency

response which depends on the distribution of harmonic force over the panel surface. Because, the complex

$$w = R \sum_{n=1}^{\infty} \sum_{m=1}^{\infty} \left\{ c_{nm} e^{(-\alpha_{nm} + \iota\omega_{nm})t} + \frac{1}{\rho_0 hR} \left[\frac{q_{nm}^+ e^{i\omega_e t}}{(\omega_{nm} - \omega_e + i\alpha_{nm})(\omega_{nm} + \omega_e - i\alpha_{nm})} + \frac{q_{nm}^- e^{-i\omega_e t}}{(\omega_{nm} - \omega_e - i\alpha_{nm})(\omega_{nm} + \omega_e + i\alpha_{nm})} \right] \right\}$$
$$\times \sin\frac{\pi n \alpha_1}{L_1} \sin\frac{\pi m \alpha_2}{L_2}, \tag{39}$$

eigenfrequency Ω_{nm} is affected by the effective complex shear modulus G being a function of induction B, the amplitude of sustained forced vibration becomes to some extent a controlled quantity. In the next section, we shall analyse the effect of an applied magnetic field on the amplitude–frequency plot for different MRE-based sandwiches.

5.2. 'Equivalent model' with external friction for the prediction of unsteady vibrations

We note that the homogeneous equation corresponding to equation (33) has the two partial solutions, $e^{-\alpha t + i\omega t}$ and $e^{\alpha t - i\omega t}$, of which the second one does not satisfy the damping condition. Thus, the general solution of equation (33) based on the above-assumed model (1) for viscoelastic MREs with internal friction cannot be used to describe unsteady forced vibrations.

In order to give an approximate analysis of unsteady vibrations, we shall replace the initial model by an 'equivalent model' with external friction. The idea of this substitution is as following: the dynamic unsteady response of the shell to the external harmonic excitation can be represented by the superposition of the damped eigenmodes and undamped forced modes of equation (34) with the wave numbers n, m. Each of the damped eigenmodes is characterized by the natural frequency $\omega_{nm} = \Re\Omega_{nm}$ and the associated damping ratio $\alpha_{nm} = \Im\Omega_{nm}$. We consider the series of viscoelastic (n, m)−oscillators

$$\ddot{y}_{nm} + 2\alpha_{nm}\dot{y}_{nm} + (\omega_{nm}^2 + \alpha_{nm}^2)y_{nm} = 0 \tag{36}$$

with the external friction and having the same eigenfrequencies ω_{nm} and damping ratios α_{nm}. Then, equation (33) may be replaced by the following equations

$$\ddot{\tilde{W}}_{ij} + 2\alpha_{ij}\dot{\tilde{W}}_{ij} + (\omega_{ij}^2 + \alpha_{ij}^2)\tilde{W}_{ij} = \frac{q_{ij}^{\pm}}{\rho_0 hR} e^{\pm i\omega_e t} \tag{37}$$

where $\tilde{W}_{ij}$ is the generalized coordinate of the 'equivalent viscoelastic system' with damping ratio α_{ij} depending on the wave numbers i, j. The partial solutions of equation (37) are the functions

$$\tilde{W}_{ij}^{\pm}(t) = \frac{q_{ij}^{\pm} e^{\pm i\omega_e t}}{\rho_0 hR(\omega_{ij} - \omega_e \pm i\alpha_{ij})(\omega_{ij} + \omega_e \mp i\alpha_{ij})} \tag{38}$$

Then, the normal unsteady response of the 'equivalent panel' to the harmonic force in equation (29) may be estimated as

where c_{nm} is the complex constant which is found from the initial conditions, and the associated displacements $\hat{u}^{(j)}$ and $\psi^{(j)}$ are determined by equation (30).

6. Dynamic characteristics of MRE-based sandwiches

6.1. Natural frequencies and damping ratios

Forced low-frequency oscillations are the most dangerous for any mechanical system because they can proceed to undesirable resonance modes. Therefore, an accurate information on the distribution of natural frequencies from the low part of spectrum for any slender structure is very important to avoid this phenomenon.

It should be noticed that for thin cylindrical shells and panels, the functional dependence of eigenfrequencies on number of waves is more complicated than that for beams and plates and strongly affected by geometrical dimensions (Mikhasev and Altenbach, 2019). So, for beams and plates, the natural frequencies are monotonically increasing functions of wave numbers. And for a thin cylindrical shell, at a fixed number n of semi-waves in the axial direction, there is such number m_* of semi-waves (waves) in the circumferential direction at which $\omega(n, m_*)$ is the local minimum. In particular, for a medium-length thin cylindrical shell closed in the circumferential direction or cylindrical panel with a large opening angle φ_2, the lowest natural frequency ω_* is reached at $n = 1$ and $m_* \sim h_*^{-1/4}$, see Mikhasev et al. (2014). This property of cylindrical sandwich-like panels is clearly demonstrated by the following

6.1.1. Example 1. Let us consider two MRE-1-based medium-length sandwiches with opening angles $\varphi_2 = \pi/3$ and $\varphi_2 = \pi$. The remaining geometrical dimensions for both sandwiches are the same: $L_2 = 1\,\text{m}$, $R = 0.5\,\text{m}$, $h_1 = h_3 = 0.5\,\text{mm}$, $h_2 = 11\,\text{mm}$. The face sheets are made of the ABS-plastic SD-0170 with the elastic properties given above and density $\rho_1 = \rho_3 = 1.04 \times 10^3\,\text{kg/m}^3$.

In Figures 4 and 5, natural frequency ω for both sandwiches is plotted as a function of induction B for different wave numbers n, m. If for the first sandwich panel with a small opening angle ($\varphi_2 = \pi/3$), the first (lowest) natural frequency is associated with the mode characterized by one semi-wave in the both directions for any induction varying from 0 to 200 mT, then for
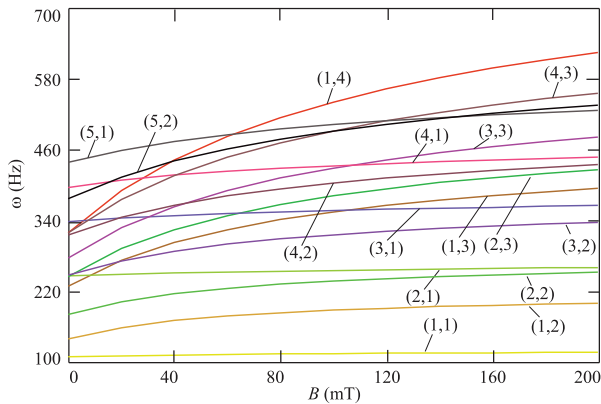
Figure 4. Natural frequency ω for MRE-1-based sandwiches with the opening angle $\varphi_2 = \pi/3$ versus induction B at different wave numbers (n, m).
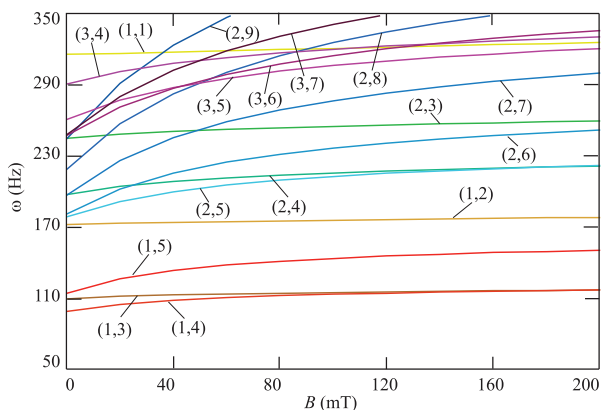

Figure 5. Natural frequency ω for MRE-1-based sandwiches with the opening angle $\varphi_2 = \pi$ versus induction B at different wave numbers (n, m).

the second panel with a large opening angle ($\varphi_2 = \pi$), the first eigenfrequency ω_* is reached at one semi-wave in the axial direction and $m_* = 4$ semi-waves in the circumferential direction, the increase of φ_2 resulting in the growth of m_*. It is also seen that for both sandwiches, there are different modes with very closed or coinciding eigenfrequencies. Due to this property, an external harmonic force may excite extensive resonance vibrations by two and more eigenmodes. Another important conclusion, following from Figures 4 and 5, is that natural frequencies are influenced by an applied magnetic field, this influence being stronger for modes with a large number of semi-waves in although one direction. For example, the natural frequency $\omega^{(1,4)}$ is changed from 300 to 600 Hz.

The next series of calculations are aimed to examine the effect of an applied magnetic field on the lowest natural frequencies and associated damping ratios for sandwiches with different thicknesses h_2 of a smart core made of different MREs.

6.1.2. Example 2. We consider five different sandwiches, S-1, S-2, S-3, S-4 and S-5, with the cores made of MRE-1, MRE-2, MRE-3, MRE-4 and MRE-5, respectively. The viscoelastic properties of these smart composite materials are given in Appendix 1. The geometrical dimensions of all the sandwiches are the same: $L_2 = 1\,\text{m}$, $R = 0.5\,\text{m}$, and $\varphi_2 = \pi$. Let the face sheets of the thickness $h_1 = h_2 = 0.5\,\text{mm}$ be made again of the ABS-plastic SD-0170.

In Figures 6–10, the lowest natural frequency

$$\omega_* = \min_{n,m} \Re\Omega(n, m) = \Re\Omega(n_*, m_*) \qquad (40)$$

and the corresponding logarithmic decrement

$$D_l = \frac{2\pi\alpha_*}{\sqrt{\omega_*^2 - \alpha_*^2}} \qquad (41)$$

where $\alpha_* = \Im\Omega(n_*, m_*)$ is plotted as a function of the magnetic field induction B at different values of h_2. For all cases, the number of waves in the axial direction is equal to $n_* = 1$, while a number m_* resulting in the minimum natural frequency depends on the core thickness h_2. For the sandwiches, S-1, S-2, S-3 and S-4, $m_* = 5, 4, 4, 4$ at $h_2 = 3, 5, 8, 11\,\text{mm}$, respectively, and for S-5, one has $m_* = 5, 4, 4, 3$ for the same sequence of thicknesses.

It is seen that for any fixed h_2, the lowest eigenfrequencies are monotonically increasing functions of the intensity of an applied magnetic field, the frequency gain being higher for sandwiches with more thick smart viscoelastic core. However, the behaviour of ω_* as a function of h_2 at a fixed B is very complicated and strongly depends on the type of an MRE embedded between elastic layers. So, for the sandwiches S-2 and S-5 assembled from MRE-2 and MRE-5, respectively, the lowest frequencies increase together with the core thickness at any induction B, while for other sandwiches the monotonic growth of $\omega_*(h_2)$ is not detected. We remind that MRE-2 is the four-parameter smart viscoelastic material, and MRE-5 with the highest content of carbon black possesses a very large shear modulus.

Interesting results are demonstrated in Figures 6(a) related to S-1: if a magnetic field is weak, then increasing a thickness of the soft MRE-1 core leads to some softening of entire packet and, in such a way, to decreasing eigenfrequencies, and the application of a strong physical field greatly increases the core stiffness and, finally, results in growing natural frequencies. Note that the increase of the magnetic field does not result in the increase of damping, in general.

As expected, the damping capabilities of all MREs under consideration are different and strongly affected by the level of an applied magnetic field and thickness of the smart core as well. For the S-5 sandwich with the MRE-5 core possessing the highest shear modulus, the logarithmic decrement D_L monotonically increases at
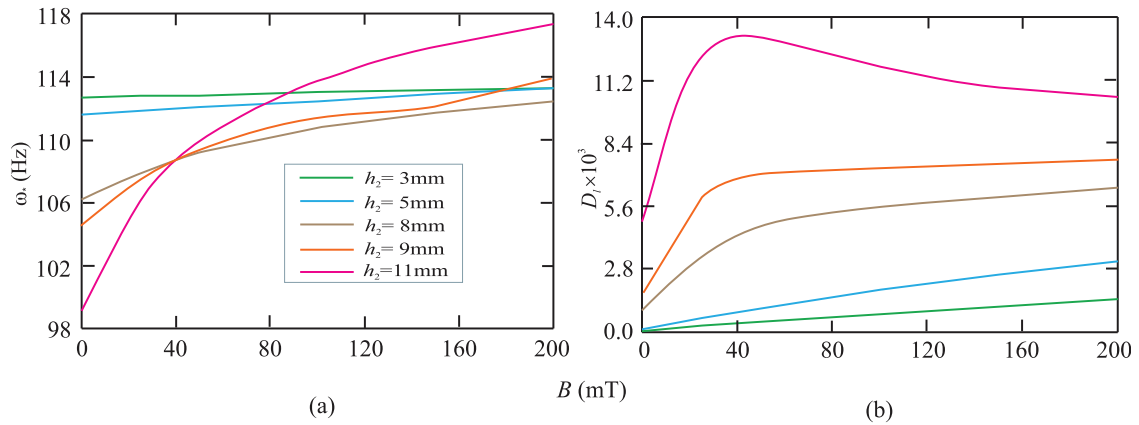
Figure 6. Lowest natural frequency ω_* (a) and associated logarithmic decrement D_l (b) for sandwich S-1 with different thicknesses h_2 of the MRE-1 core versus induction B.
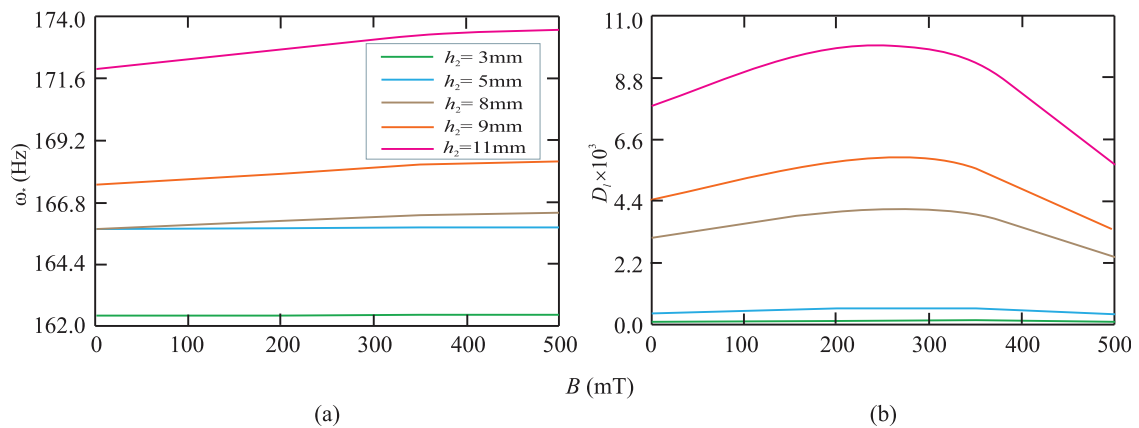

Figure 7. The lowest natural frequency ω_* (a) and the associated logarithmic decrement D_l (b) for sandwich S-2 with MRE-2 core of different thicknesses h_2 versus induction B.
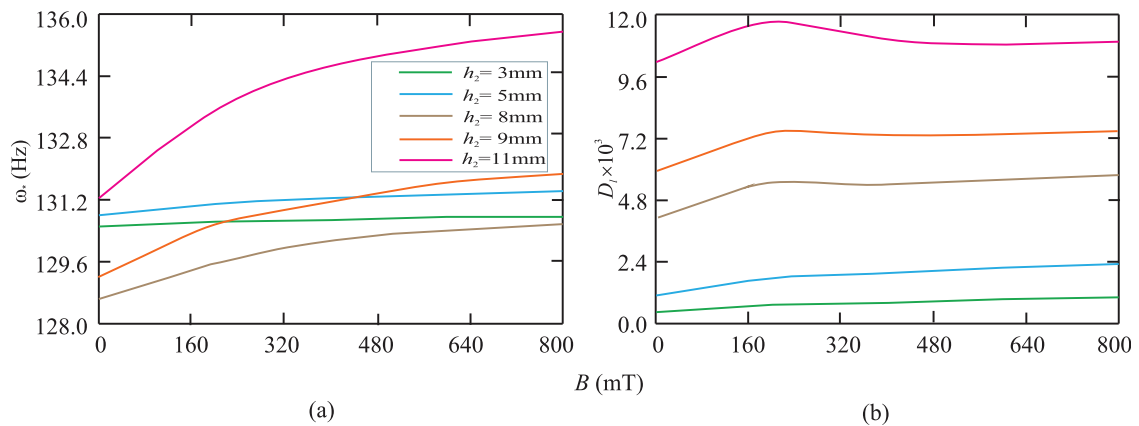

Figure 8. The lowest natural frequency ω_* (a) and the associated logarithmic decrement D_l (b) for sandwich S-3 with MRE-3 core of different thicknesses h_2 versus induction B.

all range of varying the induction B, from 0 to 800 mT (see Figure 10). The same behaviour of D_L is observed for all other sandwiches (excluding S-2) with medium and very thin viscoelastic cores. For the S-2 sandwich

with the MRE-2 core as well as for other sandwiches but with thick viscoelastic cores (at about $h_2 = 11$ mm), there are value $B = B^*$ corresponding to the yielding point for a rheological material and resulting in the
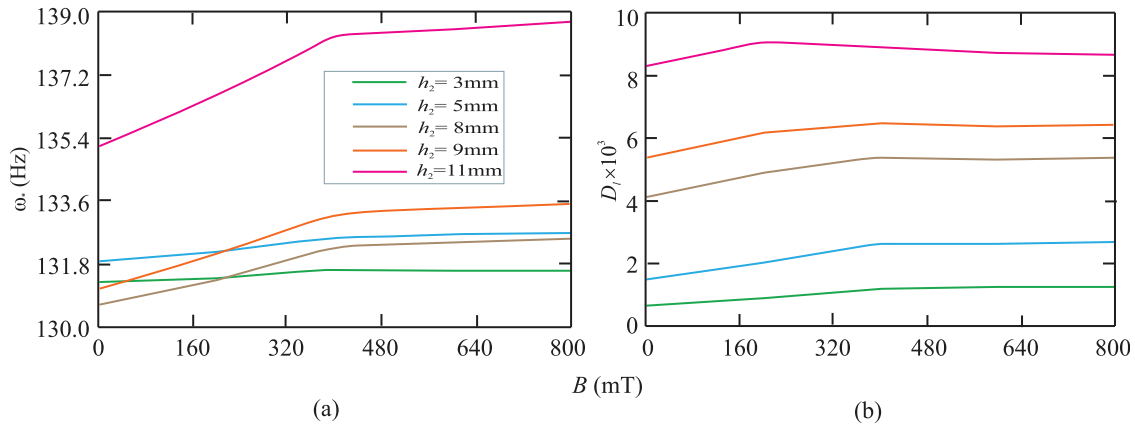
Figure 9. The lowest natural frequency ω_* (a) and the associated logarithmic decrement D_l (b) for sandwich S-4 with MRE-4 core of different thicknesses h_2 versus induction B.
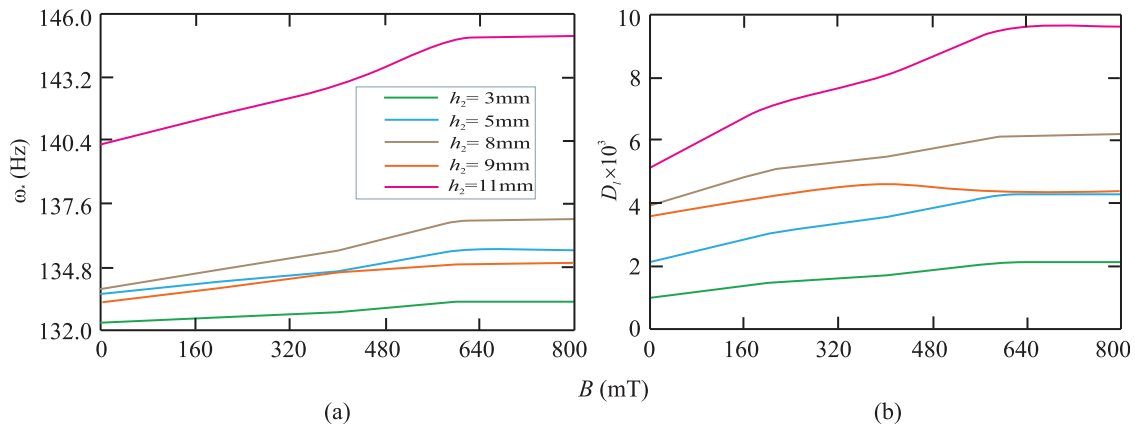

Figure 10. The lowest natural frequency ω_* (a) and the associated logarithmic decrement D_l (b) for sandwich S-5 with MRE-5 core of different thicknesses h_2 versus induction B.

maximum value of the decrement D_L. When comparing damping capabilities of all MREs at the same geometrical dimensions for sandwiches, the MRE-1 and MRE-3 reveal the highest damping properties in terms of logarithmic decrement for a sandwich.

We note that the mechanism which prevents the resonant vibrations of a smart thin-walled structure has two components. Suppression of a resonance is achieved by both shifting to the right the natural frequency at which it occurs and increasing the damping ratio. In this connection, it is of interest to compare the maximal increment of both the first frequency and logarithmic decrement with respect to the initial values without magnetic field. In Table 1, the magnitudes

$$\delta\omega_* = \frac{\max_B \omega_*(B) - \omega_*(0)}{\omega_*(0)} 100\%$$

$$\delta D_l = \frac{\max_B D_l(B) - D_l(0)}{D_l(0)} 100\%$$

are given in the numerators, while the denominators contain the value of magnetic field induction B at which

Table 1. The maximal increments $\delta\omega_*$, δD_l (%) for different sandwiches.

	S-1	S-2	S-3	S-4	S-5
$\delta\omega_*$(%)	12	0.8	3.2	2.7	3.5
B (mT)	200	500	800	800	800
δD_l(%)	60	30	13	9	51
B (mT)	40	250	230	200	700

the correspondent increment reaches a maximum. It is seen that the maximal increment of the first eigenfrequency is observed for the S-1 sandwich under the action of a relatively weak magnetic field. This effect may be explained by a high density of MRE-1 with respect to other MREs. As for the logarithmic decrement increment, it turns out to be large for both the S-1 and S-5 sandwiches (although, for the S-3 sandwich, the maximal value of D_l is larger than that for the S-5 structure); at that, for the S-1 sandwich, the high

increment of damping capability being reached at very low intensity of magnetic field.

It should be reminded that the logarithmic decrement D_l defines the decay rate of free vibrations in the one period. This magnitude, as the function of induction B, influences the suppression of the combination of damped natural modes in the general solution (39) and does not affect directly the amplitude of forced vibrations, see the last term in solution (39). It is obvious that the rate of suppression of forced vibrations depends also on the type of applied load.

6.2. Suppression of forced vibrations

To analyse the effect of suppression of forced vibrations, we consider the following

6.2.1. Example 3.
Let the sandwich S-1 with the MRE-1 core of the thickness $h_2 = 11$ mm be motionless at $t \leqslant 0$ so that

$$z|_{t=0} = \dot{z}|_{t=0} = 0 \qquad (42)$$

where z is any of displacements $w, \hat{u}_1, \hat{u}_2, \psi_1$ and ψ_2. All other geometrical dimensions as well as elastic properties of the face layers are as given above. At the time $t = 0$, the normal harmonic force

$$F = F_0 \sin \omega_e t \qquad (43)$$

is applied at the point $\alpha_1 = \alpha_1^\circ$, $\alpha_2 = \alpha_2^\circ$, where F_0 is the amplitude of concentrated force which is not specified in view of the linearity of the problem. The normal pressure q_3 per unit area can be expressed as follows

$$
\begin{aligned}
q_3 = \lim_{\substack{x_1 \to 0 \\ x_2 \to 0}} & \frac{F_0}{4x_1 x_2} \\
& \left[H_0(\alpha_1^\circ - x_1 - \alpha_1) - H_0(\alpha_1^\circ + x_1 - \alpha_1) \right] \\
& \times \left[H_0(\alpha_2^\circ - x_2 - \alpha_2) - H_0(\alpha_2^\circ + x_2 - \alpha_2) \right] \sin \omega_e t
\end{aligned}
\qquad (44)
$$

where $H_0(x)$ is the Heaviside function. Then

$$q_{ij}^{\pm} = \mp \frac{2iF_0}{L_1 L_2} \sin \frac{\delta_i \alpha_1^\circ}{R} \sin \frac{\delta_j \alpha_2^\circ}{R} \qquad (45)$$

where $i = \sqrt{-1}$, and δ_i, δ_j are determined by formula (49) of Appendix 3.

We use the above-constructed solution (39) for the panel in the framework of the 'equivalent viscoelastic model' with the external friction. The scaled amplitude A_m of the normal displacement $w(\alpha_1, \alpha_2, t)$ in the point $\alpha_1 = \alpha_1^\circ = L_1/2, \alpha_2 = \alpha_2^\circ = L_2/2$ versus time t is shown in Figure 11. The red line denotes the shell response without magnetic field, and the blue and green lines correspond to vibrations under the action of magnetic field of different intensity ($B = 40$ and 200 mT) applied at $t = 0$. The calculations were performed for the

frequency $\omega_e = 40$ Hz which is less than the lowest natural frequencies without and with a magnetic field applied. In all cases, the double infinite series in equation (30) were replaced by double finite summing up with 25 terms in each series. It is seen that without magnetic field the amplitude of oscillations being the superposition of damped natural modes remain large for a long time. The application of magnetic field results in quick suppression of these oscillations and some decreasing the component of forced vibrations, this effect turning up to be stronger at $B = 200$ mT than for $B = 40$ mT.

6.3. Amplitude–frequency characteristic

The amplitude–frequency response is very important characteristic for a thin-walled structure subjected to an external periodic excitation. Here, we shall show that varying the level of applied magnetic field, one can modify this characteristic in an MRE-based structure and considerably reduce the amplitude of resonance vibrations. For this purpose, we shall consider more examples.

6.3.1. Example 4.
Let the two S-1 sandwiches with the opening angles $\varphi_2 = \pi/3$ and $\varphi_2 = \pi$ be subjected to the concentrated harmonic force in equation (43) applied at the point $\alpha_1 = \alpha_1^\circ = L_1/2, \alpha_2 = \alpha_2^\circ = L_2/2$. All other geometrical dimensions and physical parameters are the same as in Example 3. We consider the real part of the amplitude of forced stationary vibrations calculated by equation (35) in the point $\alpha_1 = \alpha_1^\circ, \alpha_2 = \alpha_2^\circ$

$$
\begin{aligned}
w_r^\circ = & \frac{4F_0}{\rho_0 h L_1 L_2} \sum_{\substack{n=1 \\ m=1}}^{\infty} \frac{\omega_{nm}^2 - \alpha_{nm}^2 - \omega_e^2}{(\omega_{nm}^2 - \alpha_{nm}^2 - \omega_e^2)^2 + 4\alpha_{nm}^2 \omega_{nm}^2} \\
& \times \sin^2 \frac{\delta_n \alpha_1^\circ}{R} \sin^2 \frac{\delta_m \alpha_2^\circ}{R}
\end{aligned}
\qquad (46)
$$

Figure 12 shows the scaled amplitude w_r°, denoted by A_m, versus the frequency of excitation ω_e varying from 0 to 400 Hz. The amplitude–frequency plots for both sandwiches with the opening angles $\varphi_2 = \pi/3$ and $\varphi_2 = \pi$ are graphed for two different cases, without magnetic field and under its action for $B = 200$ mT. The basic conclusion following from this figure is that the application of magnetic field results in significant reduction of the amplitude of resonance vibrations. So, for the first sandwich cylindrical panel with the opening angle $\varphi_2 = \pi/3$, one has about threefold reductions for $B = 200$ mT.

It is also seen that in all cases, with and without magnetic field, for the sandwich panel with the opening angle $\varphi_2 = \pi/3$, more intensive resonance vibrations occur on the lowest (first) eigenfrequency with one
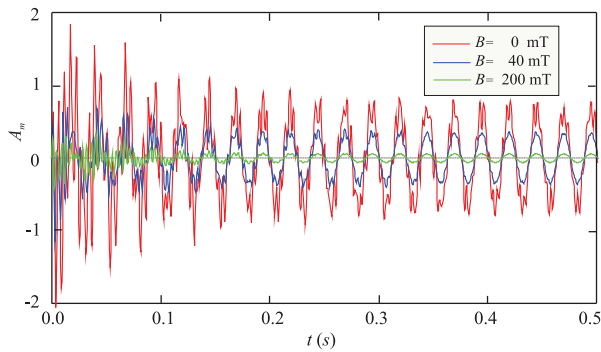
Figure 11. The scaled maximum amplitude, A_m, of forced vibrations of the sandwich S-1 versus time t at different levels of an applied magnetic field.

semi-wave in both the axial and circumferential directions ($n = 1, m = 1$), while for the panel with $\varphi_2 = \pi$, the maximum amplitude of resonance vibrations is observed due to superposition of the fifth and sixth modes with the wave numbers $n = 2, m = 5$ and $n = 2, m = 6$, respectively (see Figures 5 and 12(b)), which have very close natural frequencies. Our additional accurate calculations (their outcomes are omitted here) detected that for cylindrical panels with a small opening angle as well as for plates, the amplitude of resonance vibrations is monotonically decreasing function of a resonance frequency (at least at the low part of spectrum); while for panels with a large φ_2 as well as for cylindrical shells closed in the circumferential direction, the peak of maximum amplitude shifts to the right (at the frequency axis) and corresponds to the superposition of two or more modes with very close associated eigenfrequencies.

Also, it is of interest to note that the 'mechanisms' of suppression of resonance vibrations at the first eigenmode turn out to be different for sandwiches with small and large opening angles. As seen in Figure 12(a), applying magnetic field leads to insignificant shifting of the first resonance frequency, and the suppression occurs mainly due to enhancement of the damping capability of the smart material (here, MRE-1). As for panels with large φ_2 (see Figure 12(b)) and closed cylindrical shells as well, the action of magnetic field results in very noticeable shifting of the first resonance region to the right and about twofold decrease in the resonance peak. To appreciate this 'mechanism', one needs to apply it to Figures 4 and 5 again, the effect of magnetic field on natural frequencies turns out to be very weak for eigenmodes with small number of semi-waves n, m and increases together with these numbers.

To estimate the capability of other MREs incorporated with a sandwich panel to suppress resonance vibrations, we shall consider

6.3.2. Example 5. Let the sandwich panel S-3 with MRE-3-based core (see the property in Appendix 1) has the opening angle $\varphi_2 = \pi$. Other geometrical and physical parameters of the panel and composing layers are the same as in the previous example. We choose here the MRE-3 because the logarithmic decrement corresponding to the lowest eigenmode for the sandwich S-3 turns out to be larger (in the average for any induction B) than for other smart materials under consideration, excluding MRE-1 (compare Figures 7(b) to 10). The panel experiences the same periodic load (43) applied at the point $\alpha_1 = \alpha_1^{\circ} = L_1/2$, $\alpha_2 = \alpha_2^{\circ} = L_2/2$. Figure 13 demonstrates the amplitude–frequency response of the panel without magnetic field and under its action for $B = 200$ mT and $B = 800$ mT. It can be seen that the application of very strong magnetic field
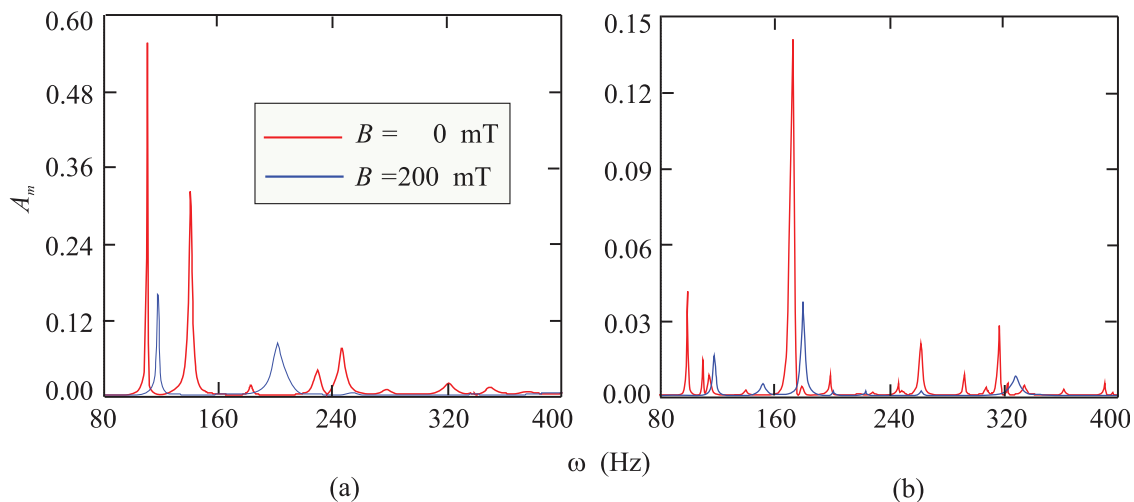

Figure 12. The amplitude–frequency characteristic for the sandwich S-1 with the opening angles (a) $\varphi_2 = \pi/3$ and (b) $\varphi_2 = \pi$ at different levels of applied magnetic field: red $-B = 0$ mT and blue $-B = 200$ mT.
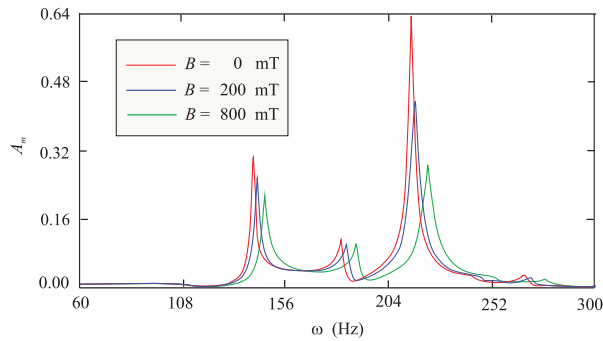
Figure 13. The amplitude–frequency characteristic for the sandwich S-3 with the opening angle $\varphi_2 = \pi$ without and with magnetic field: red $-B = 0$ mT, blue $-B = 200$ mT and green $-B = 800$ mT.

leads mainly to shifting the first and second resonance regions to the right, while the reduction of amplitudes corresponding to these regions is very weak. The noticeable lowering of the amplitude (about twofold reduction for the sandwich under consideration) is observed for the resonance vibrations on the third natural frequency, however, this reduction is reached by the application of very strong magnetic field in comparison with the sandwich S-1 (see the fifth resonance region in Figure 12(b)) subjected to more weak magnetic field. Similar calculations for other sandwiches, S-2, S-4 and S-5, and their comparison with outcomes for the S-1 sandwich revealed that the smart material MRE-1 possesses the best damping capability to suppress resonance vibrations, this suppression being provided by applying relatively weak magnetic field.

7. Conclusion

Here, we discussed the novel model of vibrations of a three-layered cylindrical panel with a core made of MRE. Such MREs can essentially change their mechanical properties under the action of magnetic field. So they can be used for control oscillations and remove some dangerous phenomena which can occur during such panels exploitation. The presented model belongs to the class of equivalent single-layer linear theory of laminated shells and generalizes the previous model proposed by Grigolyuk and Kulikov (1988). We briefly derived the basic equations of the model from the variational principle and using the generalized kinematic Timoshenko-type hypotheses. The latter are the equations of motion with respect to displacements and the corresponding boundary conditions. Here, we have restricted ourselves by considering the boundary conditions of the simple support for both straight and curved edges with diaphragms. The derived model can properly describe free and forced vibrations of a thin sandwich cylindrical panel with MRE core under the action of arbitrary external loads and magnetic field. The model used for

the analysis of vibrations of cylindrical panels for five different MREs and their applications to the vibration suppression were discussed. For assumed boundary conditions, we obtained the equation with respect to the required complex eigenfrequencies. As the equation generates additional eigenfrequencies which are not satisfied to the damping regime, we replaced the initial model with the so-called 'equivalent viscoelastic model' consisting of the set of oscillators with external friction, which results in the same spectrum of natural frequencies and associated decrements. The proposed model can be implemented to predict transient dynamic vibrations in viscoelastic cylindrical shells under the action of external non-stationary forces.

The given analysis of eigenfrequencies for MRE-based sandwich panels versus the magnetic field was confirmed earlier revealed results, namely, the applied uniform magnetic field shifts all frequencies to the right. However, this study showed that this effect strongly depends on the wave numbers. In fact, it is being very weak for modes with a small number of waves in both directions and becomes essential with the increase of the wave number in the circumferential direction. Hence, we can conclude that the low part of the natural frequencies spectrum of MRE-based medium-length thin cylindrical sandwich panels with small opening angle φ_2 is almost not influenced by even large magnetic field, while for similar panels with large φ_2, relatively weak magnetic field can considerably shift low eigenfrequencies to the right.

The five different available MREs possessing different physical properties were considered. To estimate their influence on natural frequencies and damping capability as well, we calculated the lowest natural frequencies and associated logarithmic decrements for five sandwich panels which differ only in an MRE core. The analysis of outcomes revealed that these effects are greatly dependent of the choice of an MRE, the core thickness and the magnitude of an applied magnetic field as well. For each MRE, the increase of the core thickness results in the expected growth of the logarithmic decrement. Comparing sandwiches with different MRE-based cores of the same thickness, we conclude that the sandwich containing the heavy-weight core made of MRE-1 (Korobko et al., 2012) with not very high loss factor η_v exhibits the highest increment of the first frequencies than light MREs. Also for the damping capability, MRE-1 as well as MRE-5 (with the highest content of carbon black) demonstrated very large increment in the logarithmic decrement.

In order to analyse the effect of magnetic field on forced unsteady vibrations of MRE-based sandwiches, we used the 'equivalent model' first proposed in the article. As an example, the MRE-1 based sandwich panel subjected to the action of periodic concentrated force was considered. The performed calculations showed that the application of the magnetic fields with

$B = 200\,\text{mT}$, resulted in very fast suppression of unsteady vibrations.

The amplitude–frequency characteristics plotted for two medium-length panels with different opening angles without and with magnetic field shown that for panels with a small value of φ_2 (in particular, at $\varphi_2 = \pi/3$), the maximum amplitude of resonance vibrations corresponds to the first mode with only one semi-wave in the both directions, while for panels with a large opening angle (here, $\varphi_2 = \pi$) more intensive resonance vibrations occurred simultaneously at the fifth and sixth modes with large number of semi-waves in the circumferential direction, for $n = 2, m = 5$ and $n = 2, m = 6$, respectively. It was also shown that the 'mechanism' of suppression of resonance vibrations was different for MRE-based sandwich panels of medium-length with small and large opening angles. In narrow panels with small φ_2, the application of magnetic field leads to a barely noticeable shift of the first frequencies to the right, and the resonance suppression is achieved only by enhancement of the damping capability of MRE. And for medium-length panels with large angle φ_2 as well as for medium-length cylindrical shells closed in the circumferential direction, this suppression occurs mainly because of the significant increase of the first frequencies.

The comparative calculations for different identical sandwiches differing only in MRE chosen for the core showed that from smart materials considered in the study, the MRE-1 (Korobko et al., 2012) possessed the best damping capability. In particular, in the sandwich with heavy the MRE-1 core, the satisfactory suppression of resonance vibrations is attained under application of the weak magnetic field ($B = 40\,\text{mT}$); while to achieve noticeable damping of resonance vibrations in the panel with lightweight the MRE-3 core possessing the largest loss factor, one needs to apply very strong magnetic field (about $B = 800$ mT).

The above analysis of the dynamic characteristics of thin sandwich panels with MRE core versus its geometrical dimensions, type of MRE and magnetic field applied as well indicates that design of smart thin-walled structure with the best damping properties is rather complicated multi-parametric optimization problem. This is a minimax problem which may be solved on the base of multi-parametric analysis with the chosen criteria (damping ratio, weight, magnetic field induction, etc.).

Nevertheless, our study allows making the following general important conclusions related to medium-length thin cylindrical sandwich panels containing the MRE-based core:

- For panels with a small opening angle, suppression of low-frequency free and forced vibrations is achieved mainly due to the enhancement of

damping properties and to a lesser extend because of shifting first natural frequencies; while for panels with a large opening angle it occurs due to the above two factors with emphasis on the right shifting the low part of the eigenfrequencies spectrum.

- Heavy-weight MREs like MRE-1 (Korobko et al., 2012) possessing not high loss factor but highly affecting eigenfrequencies under low magnetic field seem to be more preferable in assembling smart sandwich panels with a small opening angle; while light MREs with a large loss factors are more effective to damp low-frequency vibrations of panels with a large opening angle as well as of closed cylindrical shells.

Finally, let us remark that the presented analysis of dynamic characteristics of thin sandwich panels with different MREs may be considered as a benchmark for subsequent multi-parametric analysis and further optimal design of slender structures made of intelligent materials.

Declaration of conflicting interests

The author(s) declared no potential conflicts of interest with respect to the research, authorship and/or publication of this article.

ORCID iDs

Gennadi I Mikhasev https://orcid.org/0000-0002-9409-9210

References

Abdeljaber O, Avci O and Inman DJ (2016) Active vibration control of flexible cantilever plates using piezoelectric materials and artificial neural networks. *Journal of Sound and Vibration* 363(17): 33–53.

Aguib S, Nour A, Djedid T, et al. (2016) Forced transverse vibration of composite sandwich beam with magnetorheological elastomer core. *Journal of Mechanical Science and Technology* 30(1): 15–24.

Aguib S, Nour A, Zahloul H, et al. (2014) Dynamic behavior analysis of a magnetorheological elastomer sandwich plate. *International Journal of Mechanical Sciences* 87: 118–136.

Altenbach H (2000) An alternative determination of transverse shear stiffnesses for sandwich and laminated plates. *International Journal of Solids and Structures* 37(25): 3503–3520.

Altenbach H, Brigadnov IA and Eremeyev VA (2008) Oscillations of a magneto-sensitive elastic sphere. *Journal of Applied Mathematics and Mechanics* 88(6): 497–506.

Altenbach H, Eremeyev VA and Naumenko K (2015) On the use of the first order shear deformation plate theory for the analysis of three-layer plates with thin soft core layer. *Journal of Applied Mathematics and Mechanics* 95(10): 1004–1011.

Araújo AL, Carvalho VS, Soares CMM, et al. (2016) Vibration analysis of laminated soft core sandwich plates with piezoelectric sensors and actuators. *Composite Structures* 151: 91–98.

Babu VR and Vasudevan R (2016) Dynamic analysis of tapered laminated composite magnetorheological elastomer (MRE) sandwich plates. *Smart Materials and Structures* 25(3): 035006.

Ballhause D, D'Ottavio M, Kröplin B, et al. (2005) A unified formulation to assess multilayered theories for piezoelectric plates. *Computers & Structures* 83(15–16): 1217–1235.

Bica I, Anitas EM, Bunoiu M, et al. (2014) Hybrid magnetorheological elastomer: influence of magnetic field and compression pressure on its electrical conductivity. *Journal of Industrial and Engineering Chemistry* 20(6): 3994–3999.

Carrera E (1997) An improved Reissner-Mindlin-type model for the electromechanical analysis of multilayered plates including piezo-layers. *Journal of Intelligent Material Systems and Structures* 8(3): 232–248.

Carrera E (2003) Historical review of Zig-Zag theories for multilayered plates and shells. *Applied Mechanics Reviews* 56(2): 287–308.

Carrera E, Brischetto S and Nali P (2011) *Plates and Shells for Smart Structures: Classical and Advanced Theories for Modeling and Analysis*. Chichester: Wiley.

Chen L, Gong XL and Li WH (2008) Effect of carbon black on the mechanical performances of magnetorheological elastomers. *Polymer Testing* 27(3): 340–345.

Chikh N, Nour A, Aguib S, et al. (2016) Dynamic analysis of the non-linear behavior of a composite sandwich beam with a magnetorheological elastomer core. *Acta Mechanica Solida Sinica* 29(3): 271–283.

Choi WJ, Xiong YP and Shenoi RA (2010) Vibration characteristics of sandwich beams with steel skins and magnetorheological elastomer cores. *Advances in Structural Engineering* 13(5): 837–847.

Chróścielewski J, Kreja I, Sabik A, et al. (2011) Modeling of composite shells in 6–parameter nonlinear theory with drilling degree of freedom. *Mechanics of Advanced Materials and Structures* 18(6): 403–419.

Chróścielewski J, Schmidt R and Eremeyev VA (2019) Nonlinear finite element modeling of vibration control of plane rod-type structural members with integrated piezoelectric patches. *Continuum Mechanics and Thermodynamics* 31: 147–188.

de Souza EF, Gomes GF, Ancelotti AC, et al. (2018) Experimental dynamic analysis of composite sandwich beams with magnetorheological honeycomb core. *Engineering Structures* 176: 231–242.

de Souza EF, Gomes GF, Ancelotti AC, et al. (2019) A numerical-experimental dynamic analysis of composite sandwich beam with magnetorheological elastomer honeycomb core. *Composite Structures* 209: 242–257.

Deng H, Gong X and Wang L (2006) Development of an adaptive tuned vibration absorber with magnetorheological elastomer. *Smart Materials and Structures* 15(5): N111.

Dwivedy SK, Mahendra N and Sahu KC (2009) Parametric instability regions of a soft and magnetorheological elastomer cored sandwich beam. *Journal of Sound and Vibration* 325(4–5): 686–704.

Eisenträger J, Naumenko K, Altenbach H, et al. (2015) Application of the first-order shear deformation theory to the analysis of laminated glasses and photovoltaic panels. *International Journal of Mechanical Sciences* 96: 163–171.

Eshaghi M, Sedaghati R and Rakheja S (2015) The effect of magneto-rheological fluid on vibration suppression capability of adaptive sandwich plates: experimental and finite element analysis. *Journal of Intelligent Material Systems and Structures* 26(14): 1920–1935.

Eshaghi M, Sedaghati R and Rakheja S (2016) Dynamic characteristics and control of magnetorheological/electrorheological sandwich structures: a state-of-the-art review. *Journal of Intelligent Material Systems and Structures* 27(15): 2003–2037.

Farshad M and Benine A (2004) Magnetoactive elastomer composites. *Polymer Testing* 23(3): 347–353.

Giunta G, Biscani F, Belouettar S, et al. (2013) Free vibration analysis of composite beams via refined theories. *Composites Part B: Engineering* 44(1): 540–552.

Grigolyuk E and Kulikov GM (1988) *Multilayer Reinforced Shells: Calculation of Pneumatic Tires*. Moscow: Mashinostroenie (in Russian).

Hu B, Wang D, Xia P, et al. (2006) Investigation on the vibration characteristics of a sandwich beam with smart composites–MRF. *World Journal of Modelling and Simulation* 2(3): 201–206.

Hu GL, Guo M and Li WH (2012) Analysis of vibration characteristics of magnetorheological elastomer sandwich beam under non-homogeneous magnetic field. *Applied Mechanics and Materials* 101: 202–206.

Hu GL, Guo M, Li W, et al. (2011) Experimental investigation of the vibration characteristics of a magnetorheological elastomer sandwich beam under non-homogeneous small magnetic fields. *Smart Materials and Structures* 20(12): 127001.

Irazu L and Elejabarrieta MJ (2017) Magneto-dynamic analysis of sandwiches composed of a thin viscoelastic-magnetorheological layer. *Journal of Intelligent Material Systems and Structures* 28(20): 3106–3114.

Jolly MR, Carlson JD and Munoz BC (1996) A model of the behaviour of magnetorheological materials. *Smart Materials and Structures* 5(5): 607.

Kaplunov J, Prikazchikov DA and Prikazchikova LA (2017) Dispersion of elastic waves in a strongly inhomogeneous three-layered plate. *International Journal of Solids and Structures* 113–114: 169–179.

Kerwin EM Jr (1959) Damping of flexural waves by a constrained viscoelastic layer. *The Journal of the Acoustical Society of America* 31(7): 952–962.

Kimball A and Lovell D (1927) Internal friction in solids. *Physical Review* 30(6): 948–959.

Korobko EV, Mikhasev GI, Novikova ZA, et al. (2012) On damping vibrations of three-layered beam containing magnetorheological elastomer. *Journal of Intelligent Material Systems and Structures* 23(9): 1019–1023.

Kozlowska J, Boczkowska A, Czulak A, et al. (2016) Novel MRE/CFRP sandwich structures for adaptive vibration control. *Smart Materials and Structures* 25(3): 035025.

Kreja I (2011) A literature review on computational models for laminated composite and sandwich panels. *Open Engineering* 1(1): 59–80.

Kwon S, Lee J and Choi H (2018) Magnetic particle filled elastomeric hybrid composites and their magnetorheological response. *Materials* 11(6): 1040.

Lara-Prieto V, Parkin R, Jackson M, et al. (2009) Vibration characteristics of MR cantilever sandwich beams: experimental study. *Smart Materials and Structures* 19(1): 015005.

Li W, Zhou Y and Tian T (2010) Viscoelastic properties of MR elastomers under harmonic loading. *Rheologica Acta* 49(7): 733–740.

Li Y, Li J, Li W, et al. (2014) A state-of-the-art review on magnetorheological elastomer devices. *Smart Materials and Structures* 23(12): 123001.

Liao GJ, Gong XL, Kang CJ, et al. (2011) The design of an active–adaptive tuned vibration absorber based on magnetorheological elastomer and its vibration attenuation performance. *Smart Materials and Structures* 20(7): 075015.

Long M, Hu GL and Wang SL (2013) Vibration response analysis of MRE cantilever sandwich beam under non-homogeneous magnetic fields. *Applied Mechanics and Materials* 303: 49–52.

Megha S, Kumar S and D'Silva R (2016) Vibration analysis of magnetorheological elastomer sandwich beam under different magnetic fields. *Journal of Mechanical Engineering and Automation* 6(5A): 75–80.

Mikhasev GI, Altenbach H and Korchevskaya EA (2014) On the influence of the magnetic field on the eigenmodes of thin laminated cylindrical shells containing magnetorheological elastomer. *Composite Structures* 113: 186–196.

Mikhasev GI and Altenbach H (2019) *Thin-Walled Laminated Structures: Buckling, Vibrations and Their Suppression*. Berlin: Springer.

Mikhasev GI and Botogova MG (2017) Effect of edge shears and diaphragms on buckling of thin laminated medium-length cylindrical shells with low effective shear modulus under external pressure. *Acta Mechanica* 228(6): 2119–2140.

Mikhasev GI, Botogova MG and Korobko EV (2011) Theory of thin adaptive laminated shells based on magnetorheological materials and its application in problems on vibration suppression. In: Altenbach H and Eremeyev VA (eds) *Shell-Like Structures* (Advanced Structured Materials), vol. 15. Berlin: Springer, pp. 727–750.

Mikhasev GI, Seeger F and Gabbert U (2001) Comparison of analytical and numerical methods for the analysis of vibration of composite shell structures. In: Kasper R (ed.) *Entwicklungsmethoden und Entwicklungsprozesse im Maschinenbau, Magdeburger Maschinenbau-Tage*, vol. 5. Berlin: Logos Verlag Berlin, pp. 175–183.

Mohammadi F and Sedaghati R (2012) Nonlinear free vibration analysis of sandwich shell structures with a constrained electrorheological fluid layer. *Smart Materials and Structures* 21(7): 075035.

Naumenko K and Eremeyev VA (2014) A layer-wise theory for laminated glass and photovoltaic panels. *Composite Structures* 112: 283–291.

Naumenko K and Eremeyev VA (2017) A layer-wise theory of shallow shells with thin soft core for laminated glass and photovoltaic applications. *Composite Structures* 178: 434–446.

Nayak B, Dwivedy SK and Murthy KSRK (2011) Dynamic analysis of magnetorheological elastomer-based sandwich beam with conductive skins under various boundary conditions. *Journal of Sound and Vibration* 330(9): 1837–1859.

Nayak B, Dwivedy SK and Murthy KSRK (2012) Multi-frequency excitation of magnetorheological elastomer-based sandwich beam with conductive skins. *International Journal of Non-Linear Mechanics* 47(5): 448–460.

Nayak B, Dwivedy SK and Murthy KSRK (2014) Dynamic stability of a rotating sandwich beam with magnetorheological elastomer core. *European Journal of Mechanics-A/Solids* 47: 143–155.

Nielsen BB, Nielsen MS and Santos IF (2017) A layered shell containing patches of piezoelectric fibers and interdigitated electrodes: finite element modeling and experimental validation. *Journal of Intelligent Material Systems and Structures* 28(1): 78–96.

Prikazchikova L, Aydin YE, Erbas B, et al. (2018) Asymptotic analysis of an anti-plane dynamic problem for a three-layered strongly inhomogeneous laminate. *Mathematics and Mechanics of Solids*. Epub ahead of print 3 August 2018. DOI: 10.1177/1081286518790804.

Rajamohan V, Sedaghati R and Rakheja S (2009) Vibration analysis of a multi-layer beam containing magnetorheological fluid. *Smart Materials and Structures* 19(1): 015013.

Ross D, Ungar EE and Kervin EM (1959) Damping of plate flexural vibrations by means of viscoelastic laminae. In: Ruzicka JE (ed.) *Structural Damping*. New York: ASME, pp. 49–97.

Shaw JS and Wang CA (2019) Design and control of adaptive vibration absorber for multimode Structure. *Journal of Intelligent Material Systems and Structures* 30(7): 1043–1052.

Soroka WW (1949) Note on the relations between viscous and structural damping coefficients. *Journal of the Aeronautical Sciences* 16(7): 409–410.

Sun Q, Zhou JX and Zhang L (2003) An adaptive beam model and dynamic characteristics of magnetorheological materials. *Journal of Sound and Vibration* 261(3): 465–481.

Sun TL, Gong XL, Jiang WQ, et al. (2008) Study on the damping properties of magnetorheological elastomers based on cis-polybutadiene rubber. *Polymer Testing* 27(4): 520–526.

Tovstik PE and Tovstik TP (2016) Generalized Timoshenko-Reissner models for beams and plates, strongly heterogeneous in the thickness direction. *Journal of Applied Mathematics and Mechanics* 97: 296–308.

Wang G, Veeramani S and Wereley NM (2000) Analysis of sandwich plates with isotropic face plates and viscoelastic cores. *ASME Journal of Vibration and Acoustics* 122(3): 305–312.

Wang X, Gordaninejad F, Calgar M, et al. (2009) Sensing behavior of magnetorheological elastomers. *Journal of Mechanical Design* 131(9): 091004.

Wang Y, Hu Y, Wang Y, et al. (2006) Magnetorheological elastomers based on isobutylene–isoprene rubber. *Polymer Engineering & Science* 46(3): 264–268.

Wei KX, Meng G, Zhang WM, et al. (2008) Experimental investigation on vibration characteristics of sandwich beams with magnetorheological elastomers cores. *Journal of Central South University of Technology* 15(1): 239–242.

Yalcintas M and Dai H (1999) Magnetorheological and electrorheological materials in adaptive structures and their performance comparison. *Smart Materials and Structures* 8(5): 560–573.

Yalcintas M and Dai H (2003) Vibration suppression capabilities of magnetorheological materials based adaptive structures. *Smart Materials and Structures* 13(1): 1–11.

Yang IH, Yoon JH, Jeong JE, et al. (2013) Magnetic-field-dependent shear modulus of a magnetorheological elastomer based on natural rubber. *Journal of the Korean Physical Society* 62(2): 220–228.

Yeh JY (2011) Vibration and damping analysis of orthotropic cylindrical shells with electrorheological core layer. *Aerospace Science and Technology* 15(4): 293–303.

Yeh JY (2013) Vibration analysis of sandwich rectangular plates with magnetorheological elastomer damping treatment. *Smart Materials and Structures* 22(3): 035010.

Yeh JY (2014) Vibration characteristics analysis of orthotropic rectangular sandwich plate with magnetorheological elastomer. *Procedia Engineering* 79: 378–385.

Yildirim T, Ghayesh MH, Li W, et al. (2016) Experimental nonlinear dynamics of a geometrically imperfect magnetorheological elastomer sandwich beam. *Composite Structures* 138: 381–390.

Zhang J, Yildirim T, Alici G, et al. (2018) Experimental nonlinear vibrations of an MRE sandwich plate. *Smart Structures and Systems* 22(1): 71–79.

Zhou GY and Wang Q (2005a) Magnetorheological elastomer-based smart sandwich beams with nonconductive skins. *Smart Materials and Structures* 14(5): 1001–1009.

Zhou GY and Wang Q (2005b) Study on the adjustable rigidity of magnetorheological-elastomer-based sandwich beams. *Smart Materials and Structures* 15(1): 59–74.

Zhou GY and Wang Q (2006a) Use of magnetorheological elastomer in an adaptive sandwich beam with conductive skins. Part i: magnetoelastic loads in conductive skins. *International Journal of Solids and Structures* 43(17): 5386–5402.

Zhou GY and Wang Q (2006b) Use of magnetorheological elastomer in an adaptive sandwich beam with conductive skins. Part ii: dynamic properties. *International Journal of Solids and Structures* 43(17): 5403–5420.

Appendix I

1. *MRE-1*. This elastomer consists of a natural inorganic polymer (bentonite clay, size of

Table 2. Volume concentrations of the MRE-1 components and their densities.

MRE-1 components	Density (g/cm^3)	Weight (g)	Volume (%)
Particles of carbonyl iron	7.50	54.8	22
Bentonite clay	1.65	21.5	39
Oil 'Mobil SAE'	0.85	10.0	35
Surfactant oil	0.94	1.0	3
Total	2.63	87.3	100

MRE: magnetorheological elastomers.

Table 3. The composition of natural rubber–based MREs elaborated by Chen et al. (2008).

Sample	Magnetic particles (%)	Carbon black (%)	Matrix (%)	Density (g/sm^3)
MRE-3	33	0	67	1.895
MRE-4	33	4	63	1.872
MRE-5	33	7	60	1.855

MRE: magnetorheological elastomers.

laminar particles is 1–10 μm) in the synthetic oil and particles of carbonyl iron (particle size is about 20 μm). Densities of components and their volume concentrations for MRE-1 are presented in Table 2.

The reduced density of the MRE-1 is equal to $\rho_2 = 2.63$ g/sm^3. The MRE-1 is treated as isotropic material with Poisson's ratio $\nu_2 = 0.4$. It is the storage and loss moduli $G'_2(B), G''_2(B)$ at different levels of applied magnetic field are given in Korobko et al. (2012).

2. *MRE-2* is obtained by mixing the silicone oil and the RTV141A polymer with subsequent loading with 30% of ferromagnetic particles (Aguib et al., 2014). The density of the MRE-2 is equal to $\rho_2 = 1.1$ g/sm^3, Poisson's ratio is $\nu_2 = 0.44$, and the Young' modulus $E_2 = 1.7$ MPa is the real constant magnitude not dependent of the magnetic field induction, while $G'_2(B), G''_2(B)$ are functions of B. So, the MRE-2 is the four-parameter smart viscoelastic material.

3. *MRE-3, MRE-4*, and *MRE-5*. Table 3 shows the compositions of different natural rubber based MREs elaborated by Chen et al. (2008). For any of these elastomers, the matrix consists of the same components, 48.5% of natural rubber, 50% of plasticizers and 1.5% of other additions, but has different volume fractions due to
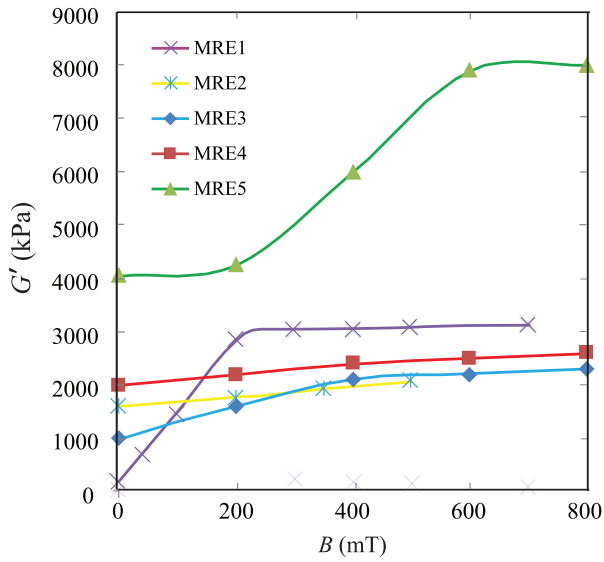
Figure 14. Moduli G_2' (kPa) versus induction B (mT) for the MREs 1–5.

Figure 15. Moduli G_2'' (kPa) versus induction B (mT) for the MREs 1–5.

introducing carbon black. The content of magnetic particles is the same and constitutes 33%.

Figures 14 to 16 reproduce the moduli $G_2'(B), G_2''(B)$ as well as the loss factor $\eta_v(B) = G_2''/G_2'$ of the MREs listed above for different values the induction B varying from 0 to 700 mT.

Appendix 2

The coefficients of equation (17) are introduced as follows

$$c_{13} = \sum_{k=1}^{3} (\zeta_{k-1} + \zeta_k)\gamma_k, \quad \frac{1}{12} h^3 \pi_{1k} = \int_{\delta_{k-1}}^{\delta_k} g^2(z)\,dz$$

$$\frac{1}{12} h^3 \pi_{2k} = \int_{\delta_{k-1}}^{\delta_k} z g(z)\,dz, \quad \frac{1}{2} h^2 \pi_{3k} = \int_{\delta_{k-1}}^{\delta_k} g(z)\,dz$$

$$\eta_1 = \sum_{k=1}^{3} \frac{\pi_{1k}\gamma_k}{\xi_k} - 3c_{12}^2, \quad \eta_2 = \sum_{k=1}^{3} \frac{\pi_{2k}\gamma_k}{\xi_k} - 3c_{12}c_{13}$$

$$\eta_3 = 4 \sum_{k=1}^{3} (\xi_k^2 + 3\zeta_{k-1}\zeta_k)\gamma_k - 3c_{13}^2$$

$$q_{44} = \frac{\left[\sum_{k=1}^{3} \left(\lambda_k - \frac{\lambda_{k0}^2}{\lambda_{kk}}\right)\right]^2}{\sum_{k=1}^{3} \left(\lambda_k - \frac{\lambda_{k0}^2}{\lambda_{kk}}\right) G_k^{-1}} + \sum_{k=1}^{3} \frac{\lambda_{k0}^2}{\lambda_{kk}} G_k$$

$$h\xi_k = h_k, \quad h\zeta_n = \delta_n \, (n = 0, k) \tag{47}$$

Appendix 3

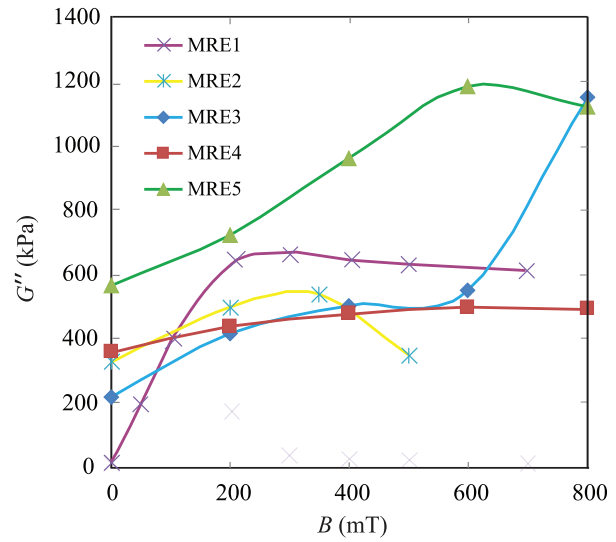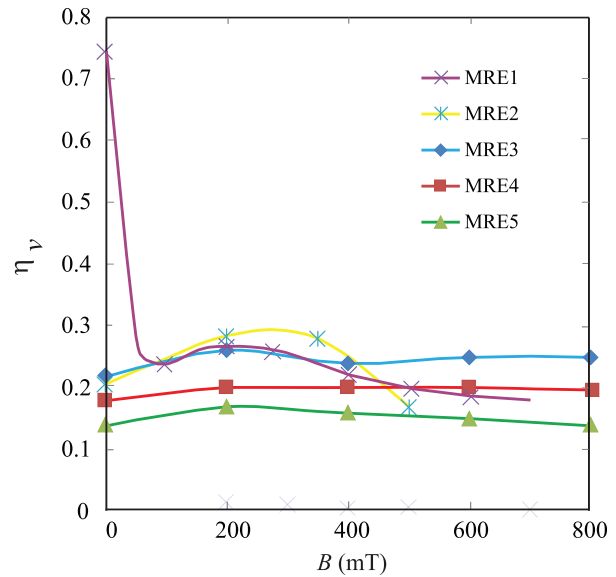The elements of the matrix **C** are given by

Figure 16. Loss factors η_v versus induction B (mT) for the MREs 1–5.

$$c_{11} = -\delta_n^2 - \frac{1-\nu}{2}\delta_m^2, \quad c_{12} = -\frac{1+\nu}{2}\delta_n\delta_m$$

$$c_{13} = \nu\delta_n, c_{14} = c_{15} = 0, \quad c_{21} = -\frac{1+\nu}{2}\delta_n\delta_m$$

$$c_{22} = -\frac{1-\nu}{2}\delta_n^2 - \delta_m^2, \quad c_{23} = \delta_m$$

$$c_{24} = c_{25} = 0, \quad c_{31} = c_{32} = 0 \tag{48}$$

$$c_{33} = \eta_2\delta_n(\delta_n^2 + \delta_m^2),$$

$$c_{34} = \eta_1\left(\delta_n^2 + \frac{1-\nu}{2}\delta_m^2\right) + \frac{q_{44}R^2\eta_3}{D}$$

$$c_{35} = \frac{\eta_1(1+\nu)}{2}\delta_n\delta_m, \ c_{41} = c_{42} = 0$$

$$c_{43} = \eta_2\delta_m(\delta_n^2 + \delta_m^2), \quad c_{44} = \frac{\eta_1(1+\nu)}{2}\delta_n\delta_m$$

$$c_{45} = \eta_1\left(\delta_m^2 + \frac{1-\nu}{2}\delta_n^2\right) + \frac{q_{44}R^2\eta_3}{D}$$

$$c_{51} = -\frac{\nu}{1-\nu^2}\delta_n, \quad c_{52} = -\frac{1}{1-\nu^2}\delta_m$$

$$c_{53} = \frac{h^2\eta_3}{12(1-\nu^2)R^2}(\delta_n^2 + \delta_m^2)^2 + \frac{1}{1-\nu^2} - \frac{\rho_0 R^2}{E}\Omega^2$$

$$c_{54} = -\frac{h^2\eta_2}{12(1-\nu^2)R^2}\delta_n(\delta_n^2 + \delta_m^2)$$

$$c_{55} = -\frac{h^2\eta_2}{12(1-\nu^2)R^2}\delta_m(\delta_n^2 + \delta_m^2)$$

$$(48)$$

where

$$\delta_n = \frac{\pi n R}{L_1}, \ \delta_m = \frac{\pi m R}{L_2} = \frac{\pi m}{\varphi_2}, \ \rho_0 = \sum_{k=1}^{3}\rho_k\xi_k \quad (49)$$

and

$$D = \frac{Eh^3}{12(1-\nu^2)}\eta_3 \quad (50)$$

is the effective bending stiffness of the laminated shell.